Dissecting the Function and Regulation of the Dual Specificity Kinase DYRK3 at the Centriolar Satellites and Primary Cilium

by

Ebru Topçu

A Dissertation Submitted to the
Graduate School of Sciences and Engineering
in Partial Fulfilment of the Requirements for
the Degree of

Master of Science

in

Molecular Biology and Genetics

August 10, 2021

Dissecting the Function and Regulation of the Dual Specificity Kinase DYRK3 at the Centriolar Satellites and Primary Cilium

Koç University

Graduate School of Sciences and Engineering

This is to certify that I have examined this copy of a master's thesis by

Ebru Topçu

and have found that it is complete and satisfactory in all respects,
and that any and all revisions required by the final
examining committee have been made.

Committee Members:

Assoc. Prof. Elif Nur Fırat Karalar (Advisor, Koç University)

Assoc. Prof. Nurhan Özlü (Koç University)

Prof. Dr. Mesut Muyan (Middle East Technical University, METU)

Date: 10th of August 2021

To my lovely family...

ABSTRACT

Dissecting the Function and Regulation of
the Dual Specificity Kinase DYRK3
at the Centriolar Satellites and Primary Cilium
Ebru Topçu
Master of Science in Molecular Biology and Genetics
August 10, 2021

The centrosome/cilium complex plays critical roles during important cellular and organismal processes. In mammalian cells, it is composed of the centrosome, the primary cilium and the centriolar satellites. At the core of the centrosome are two centrioles, which are essential for the assembly of cilia including the primary cilium, which functions as a hub for developmentally important signaling pathways. Centriolar satellites are granules that localize and move around centrosomes. These vertebrate-specific structures have emerged as important regulators of primary cilium assembly and function. Importantly, structural and functional defects of centrosomes, cilia and centriolar satellites cause various human diseases including ciliopathies, primary microcephaly and cancer. In order to uncover the pathogenesis of these diseases, a complete understanding of the mechanisms by which they are assembled, maintained and remodelled are required. To this end, I investigated the function and regulation of Dual specificity tyrosine-phosphorylation-regulated kinase 3 (DYRK3) during primary cilium assembly based on its identified in proteomic datasets of the motile cilia and regulatory functions during centriolar satellite biogenesis. First, I used proximity-based labelling approach, BioID, and generated the first in vivo proximity interaction map for wild type DYRK3 and its kinase-dead mutant. This map revealed proximity interactions between DYRK3 and regulators of primary cilium assembly and function. To test this, I inhibited DYRK3 activity in mammalian cell lines and multiciliated epithelial cultures, and showed that DYRK3 is required for primary and motile cilia assembly, respectively. These results identify DYRK3 as a new player of cilia biogenesis and advances our understanding of kinase-dependent regulation of this process.

ÖZETÇE

Sentriyolar Satelit ve Primer Silyum Konseptinde
İkili Spesifik Kinaz DRYK3'nin
Fonksiyonel ve Düzenleyici Rolunün Araştırılması
Ebru Topçu
Moleküler Biyoloji ve Genetik, Yüksek Lisans
10 Ağustos 2021

Sentrozom/Silyum kompleksi, önemli hücresel ve organismal süreçler sırasında kritik roller oynar. Memeli hücrelerinde sentrozom, primer silyum ve sentriyolar satelitlerden oluşmaktadır. Sentrozom, silyum oluşumunda gerekli olan iki adet sentriyol içerir. Primer siliyum, organismal gelişim esnasındaki önemli sinyal süreçlerinde merkez olarak işlev görür. Sentriyolar satelitler, sentrozoma localize olan ve etrafında hareket eden granül yapılardır. Bu omurgalılara özgü yapılar, primer silyumun oluşumunda ve faaliyetinde önemli düzenleyeciler olarak ortaya çıkmıştır. Sentrozom, silyum ve sentriyolar satalitlerdeki yapısal ve işlevsel bozukluklar; selyopati, primer mikrosefali ve kanser gibi insanlarda görülen çeşitli hastalıklara sebep olmaları sebebiyle önemlidir. Bu hastalıkların patogenezini ortaya çıkarmak için, bunların oluşturulduğu, korunduğu ve yeniden biçimlendirildiği mekanizmaların bütün olarak anlaşılması gerekmektedir. Bu amaçla, ikili spesifik tirozin-fosforilasyonla düzenlenen kinaz (DYRK3)'nin primer silyum oluşumu esnasındaki düzenleyici işlevini, hareketli silyum proteomik veri kümelerinde tanımlanmasına ve sentriyolar satelit biyogenezi sırasında düzenleyici işlevlere dayanarak araştırdım. İlk olarak, yakınlık temelli işaretleme yöntemi olan BioID'yi kullanarak, DYRK3 ve kinaz-ölü mutantı için in vivo yakınlık etkileşim haritasını ilk kez oluşturdum. Bu harita, DYRK3 ile primer silyum oluşum ve faaliyet düzenleyicileri arasındaki yakınlık etkileşimlerini ortaya çıkardı. Bunu test etmek için, memeli hücre hatlarında ve çoklu silyumlu epitel kültürlerinde DYRK3 aktivitesini inhibe ettim ve sırasıyla primer ve hareketli silyumların oluşabilmesi için DYRK3'nin gerekli olduğunu gösterdim. Bu sonuçlar, DYRK3'nin silyum biyogenezinde yeni bir düzenleyici olarak görev aldığını ortaya çıkardı ve bu süreçteki kinaz bağımlı düzenlenleyici rolü konusundaki anlayışımızı geliştirdi.

AKNOWLEDGEMENTS

One should appreciate the difficulties of being a member of academia. It is a full time/ lifetime job which requires a complete care and attention. In the beginning of my career as a master student, I should admit that it was not possible without psychological and physical help from others. Even though it was a tough journey, I appreciate the ones who believe in me, and there for me. Now, I am completing the one step of my career, and will start to a new one. I wish the best luck to everyone, and I hope every one of us are aware of the value we have. Do not let people make you feel insufficient, and do not forget the most important thing in life: happiness, regardless of what you are doing.

First, I would like to thank my supervisor Dr. Elif Nur Fırat-Karalar for her scientific support. I always respect her scientific enthusiasm, ideas and energy. I learned a lot of advance molecular techniques and scientific thinking thanks to her during my master studies.

Second, I would like to thank Prof. Dr. Mesut Muyan and Dr. Nurhan Özlü for accepting to be my master thesis committee member, and their comments on my work. I want to thank Mesut Muyan for his endless support from my undergraduate studies at METU to my PhD journey until now.

I acknowledge the European Research Center (ERC) (Project no: EC.00089), Scientific and Technological Research Council of Turkey (TUBİTAK) (Project no: 120N693), and Koç University for their financial support to our research during my master studies.

I would like to thank Mustafa Demir, Ahmet Kocabay, Nilhan Coşkun and Dr. Ali Cihan Taşkın for their help in Koç University Animal Research Facility and Ethics Committee (2018.HADYEK.25).

I would like to thank Koç University Proteomics Facility (KUPAM), Büşra Aytül Akarlar and Dr. Nurhan Özlü for their help for MS experiments.

I am really grateful to my lab mates Dila Gülensoy, Umut Batman, Fatmanur Tiryaki, Deniz Çonkar, Ezgi Odabaşı, Onur Taflan, Jovana Deretic, Kübra Zırhlıoğlu, Melis Arslanhan, Özge Zelal Aydın, Efe Begar, Deniz Örnek, Başak Turan, and Erdem Ercan for their support in the lab, and contributions on my data in the lab meetings. I would like to thank Umut for being my partner in science and learning many new staff together at the beginning of our master studies. I also would like to thank Esra Manka for her support in the lab.

I would like to give a special thanks to Dila, turning my Istanbul journey into something magical. Without you, my academic and social experience could not be the same.

You are the idols of my life, my mom Sevcan Topçu and my dad İlyas Topçu. I would like to thank you for always being there for me, believing in my dreams, and your endless support. I want to thank my sister Aylin Topçu, also my best friend, who always laughs with me. You always think go beyond the dreams, and inspire me with your enthusiasm towards the things that you want to achieve.

I would like to thank Ege Can Atatüre, whose support is priceless. Your rational opinions always calm me when I am overwhelmed during my thesis period. You are the one who makes the worst days into the best with your smile. Thank you for being you, and thank you for being there for me.

There have been many other people that have influenced me over my life in different ways. I would like to thank everyone who contributed to making this day happen. Thank you, my other lovely family members, my dearest friends, my professors, and people who inspires me.

TABLE OF CONTENTS

LIST OF FIGURES

ABBREVIATIONS

ALI	Air Liquid Interface
BBS4	Bardet Biedl Syndrome
BioID	Biotin Identification
BirA	Bifunctional Ligase
BSA	Bovine Serum Albumin
CCDC	Coiled Coil Domain Containing
CEP	Centrosomal Protein
CEP131	Centrosomal Protein of 131 kDa
CEP152	Centrosomal Protein of 152 kDa
CEP290	Centrosomal Protein of 290 kDa
DAPI	4',6-diaminodino-2-phenylindole
DMEM	Dulbecco's Modified Eagle Medium
DMEM-F12	DMEM/Nutrient Mixture-12
DMSO	Dimethyl sulfoxide
DYRK3	Dual specificity tyrosine-phosphorylation-regulated kinase 3
E	Empty
FBS	Fetal Bovine Serum
G0	Gap 0
G1	Gap 1
G2	Gap 2
GFP	Green Fluorescence Protein
HEK293T	Human Embryonic Kidney
HeLa	Henrietta Lacks
IFT	Intraflagellar Transport
IP	Immunoprecipitation
KD	Kinase Dead
KIF7	Kinesin-like protein KIF7
LPC	Leupeptin, Pepstatin, Chymostatin
M	Mitosis
MS	Mass Spectrometry
MTEC	Mouse Tracheal Epithelial Cells
MTOC	Microtubule Organizing Center
NSAF	Normalized Spectral Abundance Factor
OFD1	Oral-facial-digital syndrome 1 protein
P	EGFP-PCM1
P bodies	Processing Bodies
PBS	Phosphate-buffered saline
PCM	Pericentriolar Material
PCM1	Pericentriolar Material 1 Protein
PFA	Paraformaldehyde
PLK1	Polo-like kinase 1
PML bodies	Promyelocytic Leukemia Protein Bodies
PMSF	Phenylmethylsulfonyl Fluoride
RPE1	Retinal Pigment Epithelium 1
S	Synthesis

SDS-PAGE	Sodium Dodecyl Sulfate-Polyacrylamide Gel Electrophoresis
SEM	Standard Error of Mean
STLC	*S*-Trityl-L-cysteine
TBST	Tris-Buffered Saline, 0.1% Tween®
WT	Wild Type

CHAPTER 1: INTRODUCTION

The centrosome/cilium complex of mammalian cells is composed of the centrosome, the primary cilium and the centriolar satellites. The centrosome is a membraneless organelle formed from two microtubule-based cylindrical structures termed centrioles and associated pericentriolar material (PCM). The two centrioles of the centrosomes are structurally and functionally different from each other. The older of the two centrioles is known as the "mother centriole" while the younger one is called "daughter centriole". Microtubule-nucleating and organizing proteins such as gamma-tubulin docks to the centrosome and ascribes its function as the major microtubule-organizing center (MTOC) (Stearns, 2004). In interphase cells, centrosome forms radial microtubule arrays that are critical for cell migration, cell polarity and intracellular trafficking. In dividing cells, centrosomes duplicate to form the bipolar mitotic spindle, which is required for faithful segregation of genetic material to daughter cells. In quiescent cells, centrosomes move to the cell surface and nucleate the formation of the cilia including the primary cilium, motile cilia and flagellum. Given its key roles in important cellular processes, centrosome biogenesis and function are tightly regulated. In particular, centrosome duplication during cell cycle is governed by a multitude of proteins in a process called "centriole duplication cycle". Deregulation of this cycle results in centrosome number abnormalities such as supernumerary centrosomes, which is a hallmark of cancer due to its link to genomic stability and invasion (Marteil et al., 2018; Kawakami et al., 2018). Additionally, majority of the mutations that cause to primary microcephaly map to centriole duplication proteins, suggesting a tight link between regulation of this process and neurogenesis (Reiter & Leroux, 2017; Nigg & Raff, 2009).

Primary cilium is the signaling center of most animal cells. Its assembly is initiated by cellular cues such as serum deprivation and differentiation that cause cells to enter quiescence. During primary cilium formation, the mother centriole docks to the plasma membrane and acts as the basal body to template the formation of the ciliary axoneme, which protrudes to the extracellular space. Despite the progress made towards identification of the molecular players of ciliogenesis, there are still many outstanding questions that pertain to the assembly, maintenance and disassembly of the primary cilium. Importance of the centrosome components and the centriolar satellites in the

regulation of ciliogenesis are stressed out in the field by work from the Firat-Karalar laboratory and others in the field (Conkar et al., 2019; Conkar et al., 2017; Hori & Toda, 2016; Mirvis et al., 2018; Ferrante et al., 2006; Odabasi et al., 2019; Tollenaere et al., 2015; Wilkinson et al., 2009; Aydin et al., 2020). Given the important signaling functions of the primary cilium during developmental signaling pathways, its structural and functional defects has been implicated in many rare diseases and cancer (Adams et al., 2009; Hansen et al., 2011; Hildebrandt et al., 2011; Hori & Toda, 2016; Kawakami et al., 2018; Nigg & Holland, 2018; Waters & Beales, 2011).

Centriolar satellites are vertebrate-specific granular membrane-less structures that localize and move around centrosomes and cilia. Their assembly is scaffolded by pericentriolar material 1 (PCM), which interacts a wide range of different proteins implicated in centriole duplication, cilium assembly, cell division and cellular stress response. Studies from Firat-Karalar laboratory and others in the field identified the centriolar satellite interactome and showed that majority of it overlaps with the centrosome interactome, corroborating the functional and regulatory relationship between centrosomes and satellites (Arslanhan et al. 2021; Gheiratmand et al., 2019; Odabasi et al., 2019; Quarantotti et al., 2019). In line with the diversity of the satellite interactome, these structures have recently emerged as key regulators of numerous processes including primary cilium assembly and function, neurogenesis and developmental processes (Conkar et al., 2017; Mirvis et al., 2018; Nigg & Raff, 2009; Odabasi et al., 2019).

To date, a combination of genetic, proteomic, transcriptomics profiling studies in different cell types and organisms as well as functional screens have been used to identify the proteome of the centrosome/cilium complex and the proteins involved in its biogenesis and function. For example, transcriptional profile of multi-ciliated mouse tracheal epithelial cells (MTECs) were identified by Hoh et al., 2012 in order to define the proteins required for centriole amplification and motile cilia formation in this primary cell culture that recapitulates key events of differentiating tracheal epithelial cells (Hoh et al., 2012). Among the many proteins identified in the MTEC transcriptome during centriole amplification and motile cilia assembly are centriolar satellite proteins such as the core satellite proteins PCM1 and CEP131, suggesting regulatory functions for satellites in these processes.

While the above-mentioned studies defined centriolar satellites as key regulators of primary cilium and motile cilia assembly, their mechanism of action as well as context-dependent regulation remain largely unexplored. To address this question, we mined the MTEC transcriptome datasets for proteins previously implicated in centriolar satellites. Intriguingly, we found that DYRK3 was up-regulated about 20 fold at ALI-4 during centriole amplification and initiation of cilia assembly, and about 12 fold at ALI-12 during motile cilia assembly in the MTEC transcriptome data (Hoh et al., 2012). Recent work from Pelkmans at University of Zurich showed that the Dual specificity tyrosine-phosphorylation-regulated kinase 3 (DYRK3) regulates centriolar satellite biogenesis during mitosis via direct or indirect phosphorylation of PCM1 and identified DYRK3 as an important regulator of centriolar satellite biogenesis and function (Rai et al., 2018). Based on these findings, I hypothesized that DYRK3 regulates primary cilium and motile cilia assembly in part through acting on centriolar satellites. In my thesis, I combined unbiased proteomics with cellular experiments to dissect the function and regulation of DYRK3 at the primary cilium and centriolar satellites. My findings identified the first in vivo proximity interactome of DYRK3 and uncovered a previously undescribed regulatory function for DYRK3 during primary cilium assembly and length control.

1.1 Anatomy of the Centrosome

Centrosomes were first discovered in the 19th century by Edouard Van Beneden, a well-known biologist specialized on embryology and cytology (Sluder, 2014). The centrosome is a membraneless organelle that functions as the major microtubule-organizing center (MTOC) of most animal cells. It is composed of two microtubule-based cylindirical structures termed centrioles, which are structurally and functionally different from each other. The older centrioles, known as the mother centriole or basal body, has 9-fold radially arranged appendages at its distal end and using these structures, it docks to the plasma membrane during cilium assembly. The younger centriole is known as the daughter centriole, which is enriched for a set of daughter centriole proteins required for centrosome and cilium biogenesis. Centrioles are highly conserved structures that play two major roles in cells. First, they recruit pericentriolar material (PCM) to form the centrosome. Second, they template cilia assembly in quiescent cells. PCM is matrix of material surrounding the centrioles. A diverse group of microtubule-associated proteins (MAPs) including the ones required for microtubule nucleation and anchoring dock to the PCM and ascribe centrosome its functions during microtubule nucleation and organization. In addition to its well-studied functions in microtubule-dependent processes, centrosome acts as a scaffold to concentrate related proteins to mediate proteasomal degradation and thereby regulates cell fate acquisition, cell cycle control, stress response, and cell morphogenesis (Lecland & Merdes, 2018).

In interphase cells, centrosomes form the radial microtubule array required for numerous processes such as cell migration, cell polarity and intracellular trafficking. As cells enter mitosis, microtubule cytoskeleton undergoes major morphological changes where centrosomes act as the major MTOC in most cells. Like DNA duplication, centrosomes duplicate once and only once during S phase and undergo maturation during G2 phase. The duplicated centrosomes assemble the bipolar spindle during mitosis, which is required for faithful segregation of genetic material. In quiescent cells, the centrosome nucleates the cilia including the primary cilium, motile cilia and flagellum (Stearns, 2004). Defects in centrosome duplication cycle results in centriole and cilium number abnormalities that have been implicated in cancer. In particular, supernumerary

centrosomes are sufficient to cause cancer by inducing genomic instability and promoting invasive behaviour of cancer cells (Marteil et al., 2018; Kawakami et al., 2018).

The centrosome consists of a pair of centrioles surrounded by pericentriolar material (PCM). PCM is a non-membranous organelle having functions in regulating centrosome biogenesis. PCM has an important role in concentrating protein complexes that regulate protein degradation, trafficking, and spindle assembly. It should also perform cell cycle related functions since its distribution changes through the different stages, especially in cell division. In addition to its well-studied functions in microtubule-dependent processes, centrosome acts as a scaffold to concentrate related proteins to mediate proteasomal degradation and thereby regulates cell fate acquisition, cell cycle control, stress response, and cell morphogenesis (Kubo & Tsukita, 2003; Lecland & Merdes, 2018).

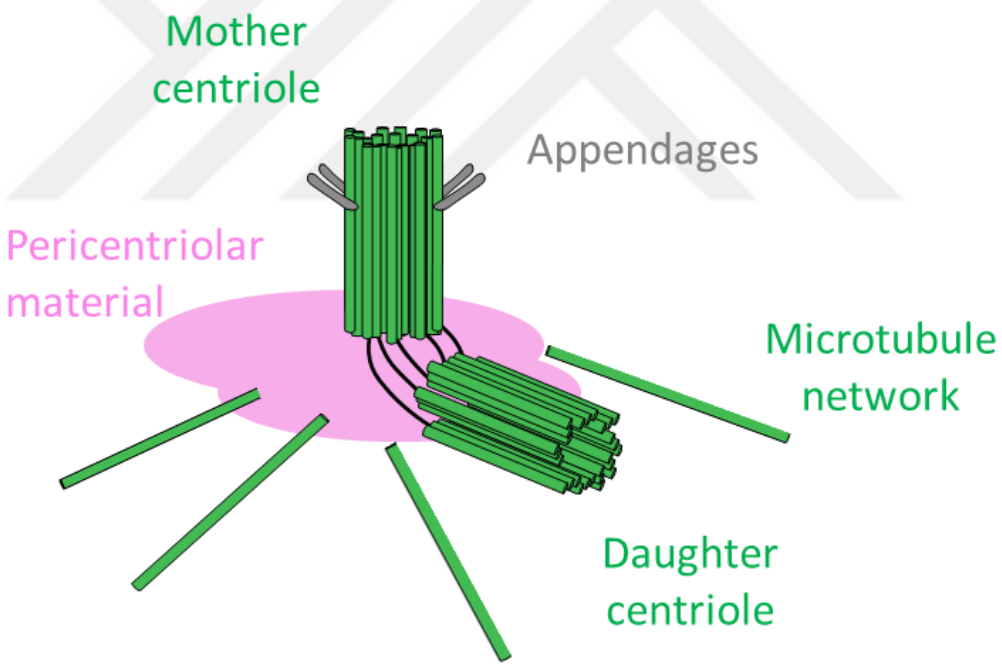

Figure 1: The anatomy of the centrosome. The centrosome is composed of two microtubule-based centrioles, one is daughter, and the other is mother. Mother centriole is the one which has distal and subdistal appendages, which are important components for cilium formation. Therefore, maternal centriole is the place that the primary cilium is nucleated. The daughter and mother centrioles are interconnected by interconnecting fibres. The centrioles are surrounded by pericentriolar material

(PCM), which is a non-membranous organelle having functions in regulating centrosome biogenesis.

1.1.1 Centrioles

Centrioles are nine microtubule triplets that are organized symmetrically in a cylinder manner. Centrioles have a typical diameter of 250 nm and a length that ranges from 150 to 500 nm, depending on the cell type and cell cycle stage (Winey & O'Toole, 2014). They are essential components to form the centrosomes, cilia and flagella in the vertebrate cells. Centrioles recruit pericentriolar material (PCM) to form centrosomes (Banterle & Gönczy, 2017).

They are microtubule-based organelles, having a triplet organization group of nine in a cylinder structure. A triplet microtubule composes of three tubules called A-tubule, B-tubule and C-tubule, and every A-tubule of a triplet is connected with the C tubule of the other triplet via a linker. Centrioles have a polar structure as microtubules, and minus ends are positioned at the proximal end of the centrioles, where the new centrioles are built forming a cartwheel structure (Winey & O'Toole, 2014).

The distinct protein composition between the maternal (distal and sub-distal appendages), and the daughter centrioles is the reflection of the functional differences in the basal body remodelling and nucleation of the cilia. The enriched proteins in the daughter centriole include CEP120, Centrobin and Neurl4, which are recruited to the daughter centriole after the centriole duplication, and removed at the next cell cycle at the maternal centriole maturation. The distal and sub-distal proteins include CEP164, CEP83, CEP89, SCLT1 and FBF1, which function in cilium assembly, Intraflagellar Transport (IFT) and vesicle docking. Additionally, sub-distal appendage proteins include OFD2, Centriolin, CEP128, CEP170 having functions in microtubule anchoring and cilium structure. The other proteins including OFD1 and C2CD3 are linked to the maturation of maternal centriole, and also localize to centriolar satellites (Wang et al., 2018).

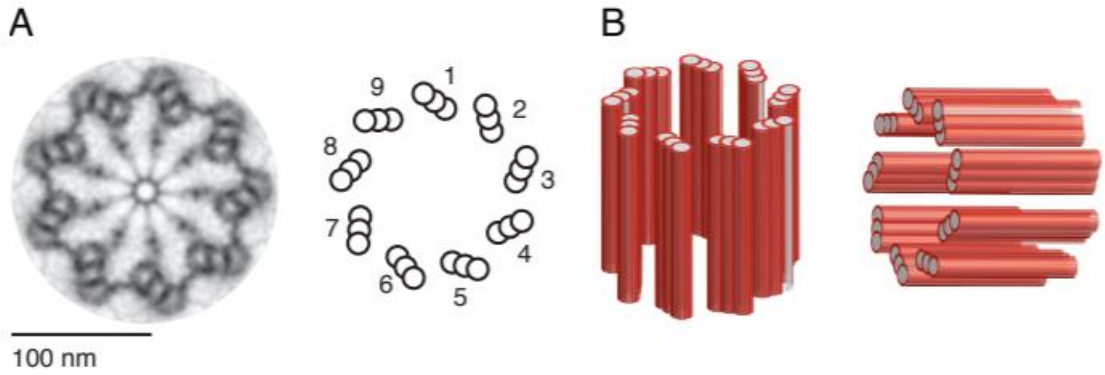

Figure 2: Nine triplet microtubule organization in the centriole structure.

A. Electron micrograph of centriole from top. Centrioles have nine microtubule triplets connecting to each other. Scale bar, 100 nm. Adapted from Gönczy, P. Towards a molecular architecture of centriole assembly. Nature Reviews Molecular Cell Biology 13, 425–435 (2012).

B. 3D representation of centrioles, as nine microtubule triplets. Adapted from Bruno, R. Quantitative analysis of centriolar satellites and control of ciliogenesis by centrosome associated kinases. PhD Thesis, Ruperto-Carola University of Heidelberg, Germany (2017).

The centriole cycle is similar with the cell cycle, and centriole duplication occurs once and only once during S-phase like DNA synthesis, and increase the centriole number from two to four during mitosis. Centriole duplication is initiated in the mother centriole, which is the older one, with the cartwheel formation. At the beginning of the duplication, PLK4 accumulates at a single focus promoting the centriole duplication in S phase, which is recruited by CEP152 and CEP192, and distributed in rings around the centriole. Gamma tubulin ring complex (gamma-TURC) nucleates the 9 tubulins along with the cartwheel, and this enables the growth of the centriole from the proximal end to distal end. When the centriole synthesis is completed, centriole disengagement occurs from M to G1 phase with the separase activity of PLK1, resulting in cartwheel disassemble. PLK1 plays a role in mitotic entry, spindle assembly, anaphase entry and cytokinesis in mitotic phase, and DNA checkpoint, chromosome condensation and centrosome maturation in interphase (Fırat-Karalar & Stearns, 2014).

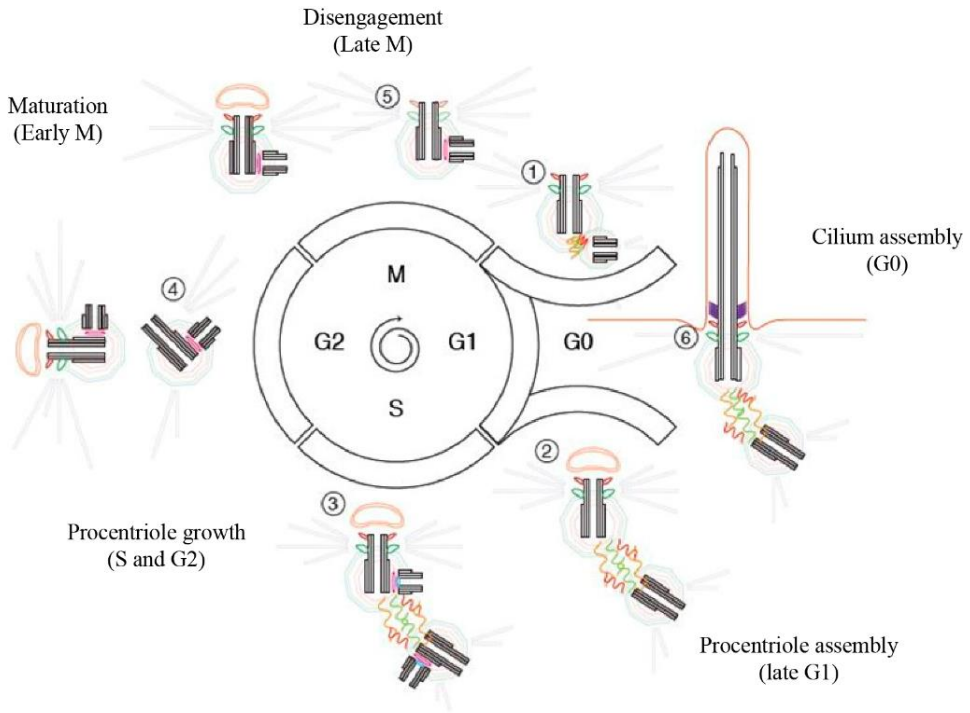

Figure 3: The Centriole Cycle. The centrosome has one maternal with distal and subdistal appendages and one daughter centriole when it is fully matured at the end of the mitosis (1). At the end of the G1, procentriole is assembled from daughter centriole and reach to the same size with the maternal centriole (2). During S phase, centrioles are duplicated as one procentriole is formed at the end of each centriole (3). The procentriole growth continues in the G2, and pericentriolar material is recruited to the centrioles (4). Connecting fibres are separated and two matured centrosomes are disengaged at the end of the M phase. The centrosomes migrate to the opposite poles of the cell, and assemble mitotic spindles on the onset of mitosis. After cytokinesis, each daughter cells have one centrosome consisting of one maternal and one daughter centrioles (5). If the cell enters to a quiescent stage, also called G0 phase, the maternal centriole becoming the basal body nucleates the primary cilium (6). Adapted from Bruno, R. Quantitative analysis of centriolar satellites and control of ciliogenesis by centrosome associated kinases. PhD Thesis, Ruperto-Carola University of Heidelberg, Germany (2017). (Bruno, 2017)

1.1.2 Pericentriolar Material

Pericentriolar material (PCM) matrix of proteins that surround the centrioles. During centrosome assembly, centrioles recruit its resident proteins and thereby play critical roles in the assembly and maintenance of PCM. PCM has an important role in concentrating protein complexes that regulate protein degradation, trafficking, and spindle assembly. It concentrates tubulin to serve the role of the primary organizing centre for microtubules in the vertebrate cells during cell division. Pericentriolar material is a place where a collection of protein complexes and nucleic acids interact dynamically, supporting its biogenesis. Core proteins in the human pericentriolar material include CEP192, CEP152, CPAP, PCNT, CDK5RAP2, PLK1 and AURKA (Woodruff et al., 2014). These proteins form ring-like structures on each other surrounding the centrioles. Therefore, PCM architecture is well-structured. During mitosis, PCM is enlarged by the accumulation of the PCM proteins, and phosphorylation of PCNT, CDK5RAP2 and CEP192 by PLK1 results the expansion. PCM expansion occurs in parallel with centrosome maturation, which is also dependent on PLK1 activity. The expansion forms an outer layer with gel-like properties resulting less stable but including core proteins for the microtubule nucleation. This increase in the nucleation capacity of PCM is necessary for spindle assembly. The limitation of the size expansion of PCM is determined by the centrosomal protein concentrations together with turnover of the PLK1 kinase activity (Fry et al., 2017).

PCM plays role in centrosome-independent functions in cell differentiation. In the differentiation, the cell enters to G0 phase, exiting from the cell cycle, and undergoes microtubule rearrangements. During this stage, the MTOC activity of centrosome is interrupted, and the cell does not nucleate microtubules from its centrosome in many cell types including epithelial, muscle and neuronal. Microtubules start to form from non-centrosomal MTOCs in the cell, which the regulatory mechanism is not well-known. The universal thing in this process is the loss of the PCM from the centrosome. It is also shown that some of the PCM components are recruited to the new non-centrosomal MTOCs in those differentiated cells. For instance, PCNT accumulates at the nuclear periphery, where microtubules are nucleated in the differentiated muscle cells.

Considering the abnormalities and disease phenotypes resulting mutations in PCM components, understanding the regulatory mechanisms is very important. In the many epithelial cancer and tumour types, high level of PCM1 is linked to disease phenotype. Additionally, mutations in PCNT, CEP152 and CPAP is identified in primordial dwarfism syndrome patients, and mutations in CEP152 and CDK5RAP2 are determined in primary microcephaly patients. Although regulation of these proteins are linked with centrosomal functions leading to defective cell divisions and apoptosis, the role of these proteins in PCM function is also related with cell division and differentiation (Fry et al., 2017; Pimenta-Marques & Bettencourt-Dias, 2020). Therefore, the importance of the PCM in the cell biogenesis and disease relations should be further investigated.

1.1.3 Centriolar Satellites

Centriolar satellites are 70-100 nm electron-dense granules that are clustered around the centrosome. They were first described by electron microscopy studies about 60 years ago and due to their pericentrosomal clustering, they were named as “centriolar satellites” (Bernhard & Harven, 1960). Like centrosomes, centriolar satellites are membrane-less macromolecular protein complexes (Kubo et al., 1999). Although they are ubiquitous in vertebrate cells, their size, distribution and number vary across different cell types and tissues. In mammalian cell lines, centriolar satellites regulate primary cilium biogenesis, composition and function, in particular its function as a signaling center during Hedgehog signaling (Odabasi et al., 2019). Work form Firat-Karalar laboratory and others in the field showed that centriolar satellites function as trafficking sites for centrosome/cilium proteins and as such, they are critical for the biogenesis and function of centrosomes and cilia (Aydin et al., 2020; Conkar et al., 2019; Odabasi et al., 2019). Due to their extensive crosstalk with centrosomes and cilia, they are accepted as the third component of the centrosome/cilium complex in vertebrate cells (Odabasi et al. , 2020).

PCM1 is the only satellite protein that interacts with all other satellite proteins and its depletion results in disintegration of satellites. Therefore, PCM1 is accepted as the molecular scaffold that is essential for satellite assembly and integrity. Because of that, PCM1 is used as universal centriolar satellite marker in immunofluorescence and

immunoblotting analysis (Kubo & Tsukita, 2003).The core components of the centriolar satellites which function in cell cycle and ciliogenesis are PCM1, CEP131, CEP290, CEP72, OFD1, BBS4, MIB1, CCDC66 and many other components and interactors are revealed (Conkar et al., 2017; Gheiratmand et al., 2019; Quarantotti et al., 2019).
Until now, various regulatory functions of centriolar satellites are revealed. Centriolar satellites are crucial component of the centrosome/ cilium complex, and have important roles in cilium assembly (Conkar et al., 2017; Wang et al, 2016), centrosome duplication (Fırat-Karalar & Stearns, 2014; Kodani et al., 2015), microtubule regulation and chromosome segregation (Kim et al., 2012). Apart from ciliogenesis and cell division functions, the role of centriolar satellites in the stress response (Villumsen et al., 2013), autophagy (Pampliega et al., 2013; Tang et al., 2013) and neurogenesis (Tollenaere et al., 2015) are also determined. Additionally, proteins mutated in primary microcephaly, ciliopathies and neurological disorders are components of satellites and their centrosomal targeting were shown to be regulated in part by satellites (Kodani et al., 2015). These lines of evidence corroborate functions of satellites during development and differentiation. Additionally, centriolar duplication proteins also localize to satellites, suggesting a link between satellites and cancer caused by centriole number abnormalities.

Although recent studies uncovered functions and molecular mechanisms of centriolar satellites in cells, the mechanisms that regulate their biogenesis remain largely unexplored, which limits our understanding of their disease links. Regarding their assembly and integrity, it is known that PCM1 is essential as a scaffolding protein. Additionally, recent work highlighted the importance of posttranslational modifications in centriolar satellite assembly and distribution. For example, the master regulator of centriole duplication PLK4 localizes to satellites, phosphorylates PCM1 and regulates satellite distribution and dynamics (Hori et al., 2016) Additionally, inhibition of DYRK3 was shown to inhibit centriolar satellite dissolution during mitosis and thereby it resulted in prolonged mitosis, suggesting regulatory functions for satellites during cell cycle progression (Rai et al., 2018).

1.1.4 Tissue Specific Regulation of Centriolar Satellites

Centriolar satellites (PCM1) are differentially distributed among the different cell types. Their cellular distribution is changed from accumulating to the centrosome, around nucleus or basal bodies to distributing among the cytosol (Kubo & Tsukita, 2003; Odabasi et al., 2020; Srsen et al., 2009; Vladar & Stearns, 2007). In the vertebrate epithelial cells, centriolar satellites are observed around the centrosome, and the basal body in the ciliated cells. During the differentiation of in vitro mouse tracheal epithelial cells (MTECs), satellites are observed as fibrous granules in close to amplified centrioles after air liquid interface (ALI) introduction. They are distributed at the below portion of the basal bodies which are located at the apical surface in the multi-ciliated cells. In the neuronal cells, centriolar satellites are distributed along the axon and the dendritic branches. In the muscle cells, they are distributed around the nuclear envelope, which is a non-centrosomal microtubule organizing centre (Kubo & Tsukita, 2003; Odabasi et al., 2020; Sanchez & Feldman, 2017; Srsen et al., 2006; Vladar & Stearns, 2007). Their differential distribution in the different cell types and tissues suggests tissue specific functions of centriolar satellites.

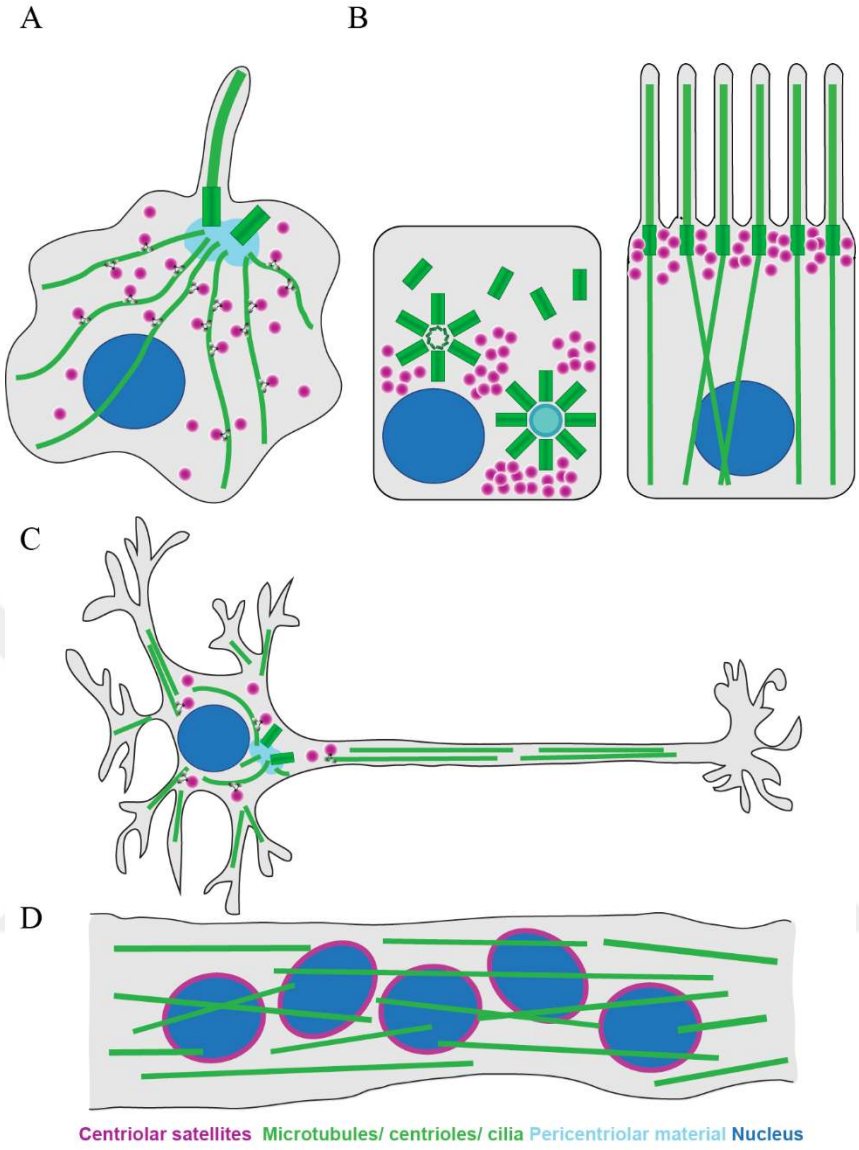

Figure 4: Distribution of centriolar satellites changes in different cell types and tissues.

A. Centriolar satellites are distributed mainly around the basal body in the ciliated cells, and move along the microtubules throughout the cell.

B. Centriolar satellites are remodelled during the differentiation of MTECs. They form fibrous granules in the close proximity to centrioles in the centriole amplification stage. After induction of air-liquid interface (ALI), satellites are accumulated at the below part of the centrioles that dock into the apical surface.

C. Centriolar satellites are distributed along the cell body of the neuronal cells.

D. Centriolar satellites accumulates at the nuclear periphery of the differentiated muscle cells.

Adapted from Odabasi, Batman & Firat-Karalar, 2020. Unravelling the mysteries of centriolar satellites: time to rewrite the textbooks about the centrosome/cilium complex, Molecular Biology of the Cell, Vol.31, No.9.

1.1.5 Mitotic Regulation of Centriolar Satellites

Centriolar satellites are differentially distributed among the different cell cycle stages. They are accumulated on the duplicated centrosomes in prometaphase, and spindle poles in early metaphase. They dissolve during the later stages of the mitosis increasing their cytoplasmic pool, and decreasing the granules. Centriolar satellites go through remodelling in an extensive manner upon cell cycle and various range of cellular stress factors. They should also perform cell cycle related functions since its distribution changes through the different stages, especially in cell division. Although their mitotic dissolution, their total protein level is not much affected. Most of them re-localize to centrosome or cytoplasm during mitosis, and it is thought that this is regulated by the post-translational modifications (Rai et al., 2018; Tollenaere et al., 2015). During the mitotic regulation of centriolar satellites, they undergo fission and fusion events, resemble to liquid-like behaviour of the proteins (Banani et al.2017; Conkar et al., 2019). Remodelling of centriolar satellites during mitosis is shown to be regulated by the dual specificity tyrosine kinase DYRK3, which is defined as the central dissolvase of several membraneless organelles including stress granules and P-bodies (Rai et al., 2018). In the inhibition of the DYRK3, they observe that the number of PCM1 granules are increased, and the inhibition of DYRK3 and the overexpression of the kinase dead version fail to dissolve PCM1 during mitosis, comparing with the wild type version. However, this effect is dependent on the concentration of the active kinase, and the effect of the endogenous level DYRK3 needs to be elucidated (Rai et al., 2018). There are many questions to be answered in the regulation of centriolar satellites during mitosis including the post-translational modifications and the liquid-liquid like phase separation behaviours.

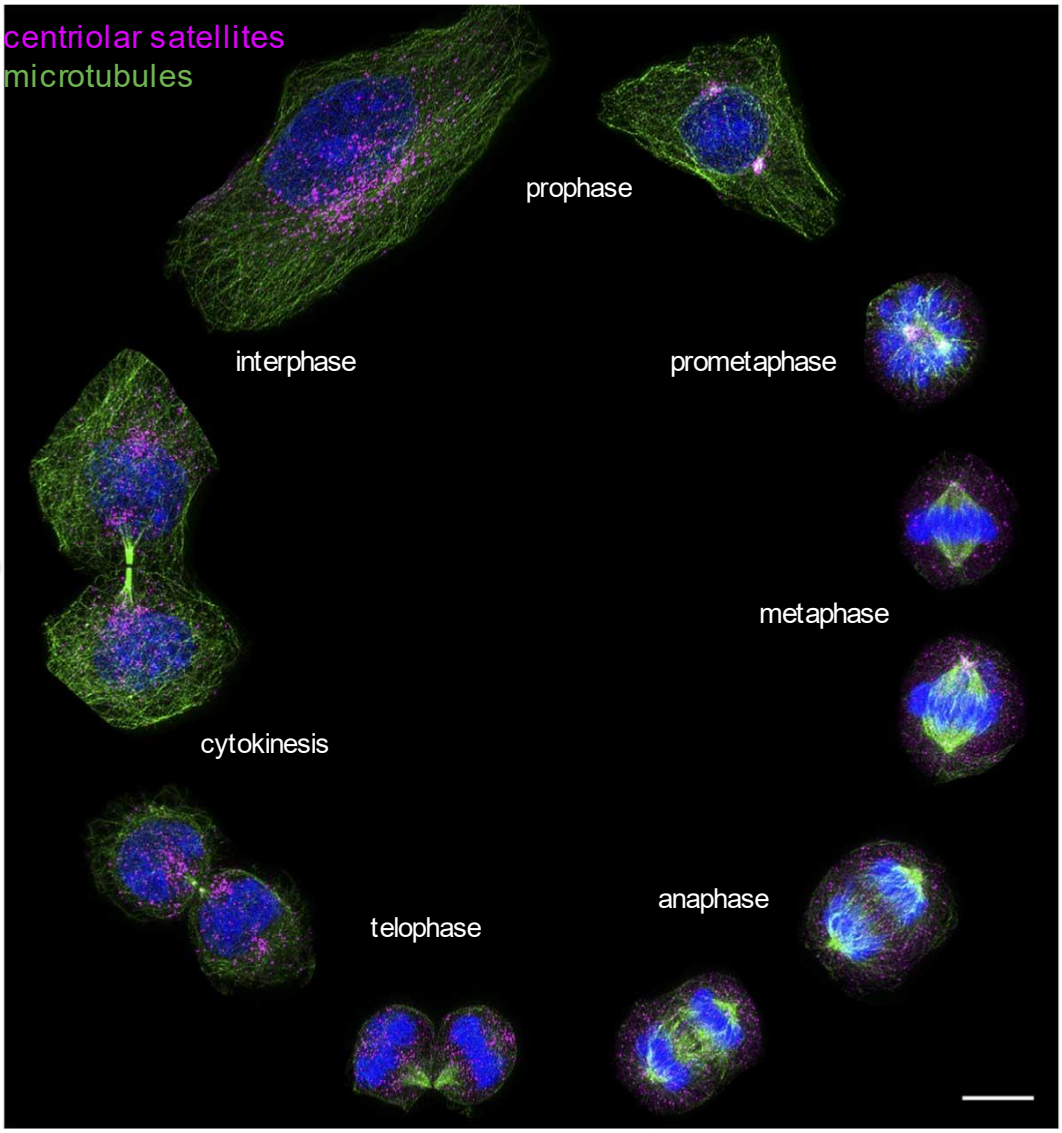

Figure 5: Centriolar satellite distribution changes during cell cycle. Localization of centriolar satellites is shown in different stages of the cell cycle in HeLa cells. The cells are immunostained in different stages using antibodies against PCM1 for centriolar satellites (magenta) and a-tubulin for microtubules (green), and DAPI for DNA (blue). Satellites are concentrated on basal bodies and spindle poles at prometaphase and metaphase respectively. They are dissolved during mitosis increasing their cytoplasmic pool. After cytokinesis, they relocalize close proximity to the centrosome and distributes along with the microtubules. Scale bar, 10 um. Adapted from Odabasi, Batman & Firat-Karalar, 2020. Unravelling the mysteries of centriolar satellites: time to rewrite the textbooks about the centrosome/cilium complex, Molecular Biology of the Cell, 31, 9.

1.1.6 Regulation of Centriolar Satellites on Ciliogenesis

The composition and distribution of centriolar satellites are altered during the cilium assembly. The centriolar satellite components that are also implicated ciliogenesis are redistributed onto basal body and cilium (Akiko Hori & Toda, 2016). One determined function of centriolar satellites on ciliogenesis is the cilium assembly, and alterations in many of them disrupt the ciliogenesis. One suggestive regulation mechanism is the trafficking regulation of ciliary components, considering their dynamic movement along with the motors on the microtubules (Conkar & Firat-Karalar, 2020). Another evidence of the centriolar satellite function and regulation on ciliogenesis is the BBSome component protein BBS4, which localizes to centriolar satellites in interphase cells, but redistributed to the primary cilium in the quiescent cells (Nachury et al., 2007). Depletion of some satellite components like PCM1, CCDC66, CEP72 and CEP290 is shown to ablate ciliary recruitment of the important ciliary components resulting ciliogenesis defects (Conkar et al., 2017; Hoh et al., 2012; Nachury et al., 2007; Odabasi et al., 2019). Additionally autophagy-induced degradation of OFD1, a core component of centriolar satellites was shown to induce ciliogenesis (Tang et al., 2013). Their redistribution onto apical surface in differentiation of multi-ciliated epithelial cells also gives cues on regulatory functions of satellites on ciliogenesis (Sorokin, 1968; Kubo et al., 1999; Vladar & Stearns, 2007). The function and regulation of centriolar satellites on ciliogenesis needs to be further elucidated considering the disease relations and abnormalities in the disruption of the ciliogenesis in the cells and the tissues.

1.2 Cilia

Cilia are classified into the non-motile primary cilium and the motile cilia. Primary cilium is present in most animal cells except for the specialized epithelial that have hundreds of motile cilia on the surface and flagellum of sperm. Primary cilium is a microtubule-based organelle that protrudes as one copy from the surface of most animal cells in order to sense signals important for homeostasis and thereby behaves as the cellular ‘antenna’. The ciliary axoneme is, templated by the basal body, which is surrounded by the ciliary membrane. Primary cilium biogenesis is tightly linked to cell cycle. Its assembly is

induced in quiescent cells by serum starvation or differentiation signals. As cells enter mitosis, primary cilium disassembles (Malicki & Johnson, 2017).

The primary cilium is composed of nine doublets of microtubules, and projects out of the cell surface via its axoneme. It is noted that cilia structure and function can vary depending on the organism and the cell type. There are two main types of the cilia: primary cilia and motile cilia. In the motile cilia, axonemal microtubules are decorated with dynein complexes to achieve ciliary movement, and motile cilia have an extra central microtubule doublet. Therefore, motile cilia microtubules are called 9 + 2 arrangement in the comparison with the 9 + 0 arrangement of the primary cilia. Structurally, each cilium comprises a microtubular backbone known as the ciliary axoneme, which is surrounded by plasma membrane. Primary cilia appear typically as single appendage microtubules on the apical surface of cells and lack the central pair of microtubules (Mirvis et al., 2018).

Primary cilium composition is tightly regulated to ensure its proper function as the signaling center. Given that primary cilium does not have ribosomes, ciliary proteins are synthesized in the cell body and transported to the cilium. Ciliary transport is achieved by Intraflagellar Transport (IFT), an ordered and highly regulated anterograde and retrograde translocation of polypeptide complexes (IFT particles) along the length of the ciliary axoneme (Ishikawa & Marshall, 2011). In addition to the IFT complex, cilium complex is regulated by various other processes such as the transition zone that functions as a gate for entry to and exit from cilium and extracellular vesicles that are secreted from the tip of the cilium (Conkar & Firat-Karalar, 2020).

Given the important functions of cilia in motility and signaling, defects in their structure and function cause numerous human diseases including developmental disorders and cancer. Primary cilium is critical in receiving and transmitting developmentally important signaling pathways such as Hedgehog, Wnt and PDGFR signaling. As such, their defects cause sensory ciliopathies that are characterized by multisystemic developmental disorders such as retinal degeneration, polycystic kidney disease, polydactyly among others (Adams et al., 2009; Nigg & Raff, 2009). As for motile cilia, their deregulation causes motile ciliopathies characterized by respiratory problems, hydrocephaly and infertility (Hansen et al., 2011; Reiter, 2017; Juhler, 2012; Waters & Beales, 2011; Wei

et al., 2018). Finally, supernumerary cilia were proposed to contribute to cancer phenotypes by disrupting transmission of signaling pathways (Marteil et al., 2018; Kawakami et al., 2018; Nigg & Holland, 2018). To elucidate the pathogenesis of these diseases, it is essential to have a complete understanding of cilium structure, function and regulation.

1.2.1 Primary Cilium Assembly

Primary cilium biogenesis is tightly linked to cell cycle. Its assembly is initiated in quiescent G0 cells induced by cellular cues such as cellular stress, differentiation and serum starvation. As cells enter mitosis, primary cilium disassembles via deacetylation of the axoneme. During ciliogenesis, mother centriole transforms into the basal body to template nucleation of ciliary axonemes. The daughter centriole is connected by fiber rootlets from their proximal ends. The basal body is connected to the plasma membrane of the apical surface by transition fibers originated from the distal appendages. At the top portion of the basal body, primary cilium is composed of three main portions, which are the transition zone, axoneme and ciliary tip. The transition zone contains Y-links connecting the microtubule doublets of the ciliary axoneme to the ciliary membrane. The transition zone behaves as a diffusion barrier for the entry and exit of the ciliary components. The ciliary tip is the place for turnover of the Intraflagellar Transport components, Hedgehog signaling, microtubule assembly and disassembly, and ectocytosis (Conkar & Firat-Karalar, 2020; Ishikawa & Marshall, 2011; Mirvis et al., 2018).

During initiation of the primary cilium assembly, the nine triplets of the maternal centriole are remodelled to nine microtubule doublets (A- and B- tubules) at the distal end of the basal body supporting the ciliary axoneme architecture. Along with the axoneme, the well-structured 9 + 0 structure is lost, and microtubules start to twist each other eliminating the A- and B- tubule numbers towards the ciliary tip. Therefore, the diameter of the axoneme is decreased starting from around with a 0.2 um diameter, and it is narrowing along the axoneme and the tip (Sun et al., 2019) . The cilium assembly is a regulated process and associates the basal body with periciliary vesicles from the Golgi

apparatus and initiates the axoneme maturation. The vesicles are then fused to form the ciliary membrane along with the plasma membrane. Axoneme elongation are achieved by the transport of the tubulin and IFT proteins enabling the trafficking of signalling and structural components of the cilium (Nakayama & Katoh, 2018). At the time when the basal body docks into the plasma membrane by distal appendages, the cilium protrudes from the cell surface and the cilium is assembled (Wang et al., 2018). The ciliogenesis capacity and the cilium length differ depending on the cell type and tissues. In general, the primary cilium length varies from 1 to 5 um (Conkar & Firat-Karalar, 2020; Scherft & Daems, 1967).

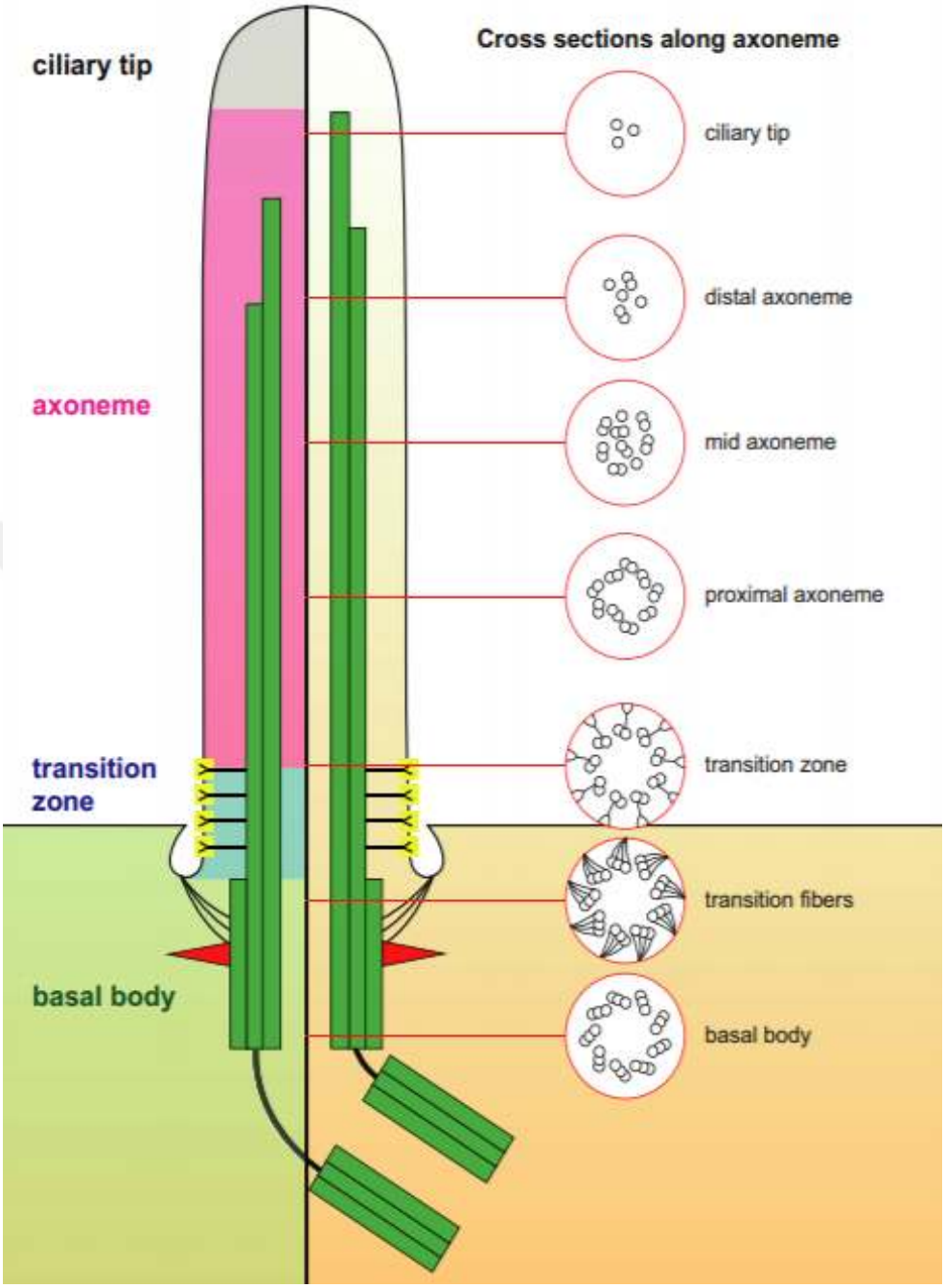

Figure 6: The anatomy of the primary cilium. The structures and the architecture components of the vertebrate primary cilium. The primary cilium is nucleated from the maternal centriole forming the basal body with the formation of accessory components distal and sub-distal appendages. Transition fibers connect the basal body to the cell surface supporting the cilium shape. The forming cilium consists of three main parts which are transition zone, axoneme and ciliary tip. Y-links in the transition zone connects the microtubule doublets of the ciliary axoneme to the ciliary membrane. The nine triplets of the maternal centriole are remodelled to nine

microtubule doublets (A- and B- tubules) at the distal end of the basal body, so that the well-structred 9 + 0 structure is lost, and microtubules start to twist each other eliminating the A- and B- tubule numbers towards the ciliary tip. Therefore, the diameter of the axoneme is narrowed towards the ciliary tip. Adapted from Conkar & Firat-Karalar, 2020. Microtubule-associated proteins and emerging links to primary cilium structure, assembly, maintenance, and disassembly, FEBS Journal, 288, 3, 786-798.

1.2.2 Multi-ciliation

Multi-ciliated epithelial cells are terminally differentiated cells that have hundreds of motile cilia, which are microtubule-based organelles important for the liquid movement in the respiratory tract, brain ventricles and reproductive tracts in the mammals. The motile cilia of the multi-ciliated cells beat synchronously to move liquid and particles such as mucus in tracheal cells and eggs in fallopian tube. Accordingly, defects in their structure, number and motility causes motile ciliopathies characterized by respiratory problems, hydrocephalus, infertility, and left-right asymmetry during embryonic development (Brooks & Wallingford, 2014; Nanjundappa et al., 2019; Stubbs et al., 2012).

The formation of the multi-cilia starts with the centriole amplification process to generate hundreds of centrioles. Mainly, there are two parallel pathways for centriole amplification in the multi-ciliated cells. One is the canonical centriole duplication pathway, and the other is the deuterosome pathway. The canonical parental pathway includes the parental centrioles as a template, and following the assembly of the many procentrioles at the same time. Differently, deuterosome pathway is a de novo pathway mediated by many deuterosomes, and one deutresome is capable of the assembly of many procentrioles. They are temporary structures that form during early centriole amplification, and not observed in the proliferating cells (Nanjundappa et al., 2019). These procentrioles are not accumulated around the maternal centriole, rather emerge in an unexceptional way as electron-dense barrel shape structures called deutresomes (Klos Dehring et al., 2013).

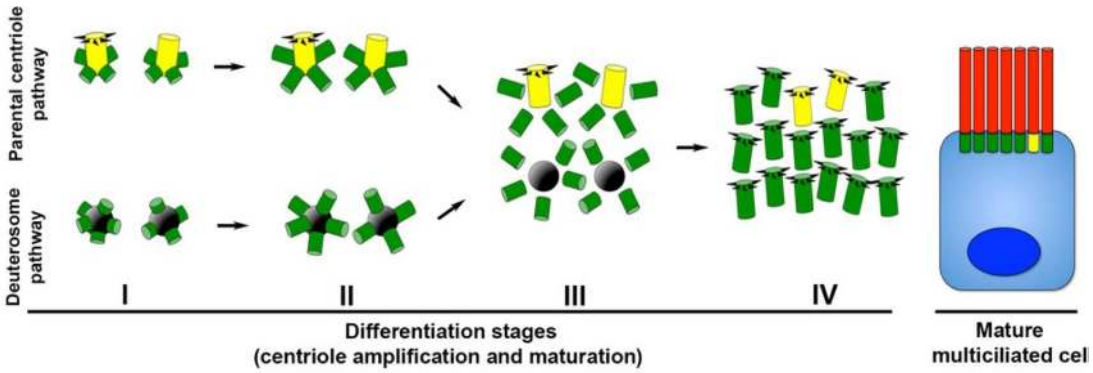

Figure 7: Multi-ciliation occurs via two pathways. Parental centriole and deuteresome pathways form multi-ciliated cells during cellular differentiation. These pathways are interconnected and occurs simultaneously. Parental centrioles are shown in yellow, deuterosome mediated procentrioles are in green, and cilia is in red. Adapted from Nanjundappa, Kong, Shim, Stearns, Brody, Loncarek & Mahjoub, 2019. Regulation of cilia abundance in multiciliated cells, eLife;8:e44039.

CHAPTER 2: DISSECTING THE FUNCTION AND REGULATION OF THE DUAL SPECIFICITY KINASE DYRK3 AT THE CENTRIOLAR SATELLITES AND PRIMARY CILIUM

2.1 DYRK Family Kinases

Dual specificity tyrosine phosphorylation regulated kinases (DYRKs) are a group of kinases characterized for their function during signal transduction, cell proliferation and survival, and cell differentiation. Protein kinases mediate their functions during signal transduction processes by phosphorylation or dephosphorylation of a diverse array of substrates. Deregulation of their activity results in defects in signal transduction pathways and thereby various disease phenotypes that correlate with the cellular and organismal functions of the specific signaling pathway they are involved in. Protein kinases are classified according to their homology and function, which include Tyrosine kinases, tyrosine-like kinases, Calcium/calmodulin dependent kinases (CAMK, Cyclin dependent kinases (CDK), Mitogen activated protein kinases (MAPK), and Glycogen synthase kinase (GSK3) and CDC-like kinase (CLK) group of protein kinases (CMGC) (Singh & Lauth, 2017).

CMGC protein kinases is divided into nine families including CDK, CDKL, GSK, CLK, MAPK, HIPK, DYRK, RCK and SRPK kinases. Members of this kinase family is highly conserved among the evolution from nematodes to humans. The CMGC group of kinases have a range of functions such as signal transduction, cell cycle, RNA biogenesis and intracellular signaling. Among the members of the CMGC kinase family, MAPKs and CDKs are the most studied groups due to their relation to cancer. In comparison, DYRKs have remained as poorly characterized CMGC kinase family members until the discovery of their key functions in regulation of liquid-liquid phase transition (Rai et al., 2018; Singh & Lauth, 2017).

There are five members of DYRK family kinases in mammalian cells, which all contain a characteristic sequence motif called the DYRK homology box (DH box), next to their kinase sequence. DYRK family kinases are conserved from yeast to humans. They are divided into two subgroups which are Class I and Class II. Class I includes DYRK1A and

DYRK1B, and Class II includes DYRK2, DYRK3 and DYRK4. These classes are classified based on their additional sequence homologies. DYRK1A and DYRK1B have a PEST domain which is a motif rich in proline, glutamate, serine, and threonine amino acids. Both have nuclear localization signals (NLS), but DYRK1A has also a second NLS in its kinase motif. Additionally, DYRK1A has one poly-histidine stretch (HIS), and a serine/threonine rich region (S/T). Distinct motif for Class II is a N-terminal auto-phosphorylation accessory region (NAPA). DYRK2 and DYRK4 also have NLS, but not DYRK3 (Singh & Lauth, 2017).

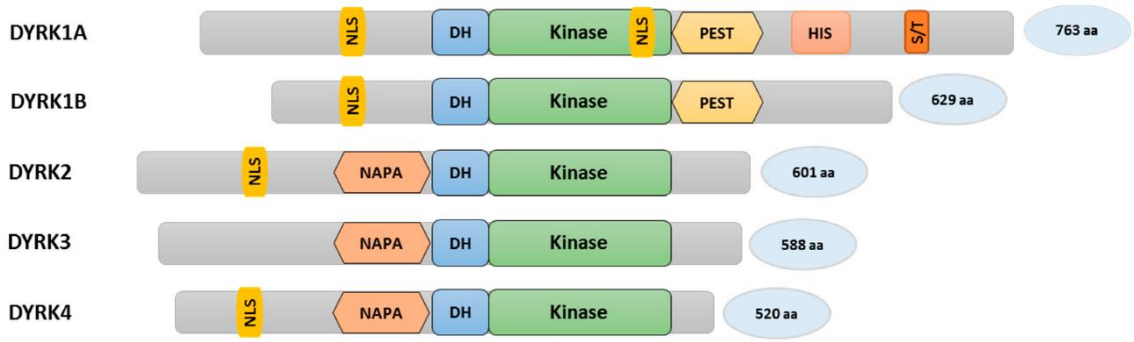

Figure 8: Domain representations of Class I and II DYRK family kinases. All five members of the DYRK family kinases contain a characteristic sequence motif called the DYRK homology box (DH box), next to their kinase sequence. The Class I members, DYRK1A and DYRK1B have a motif rich in proline, glutamate, serine, and threonine amino acids (PEST domain). All have nuclear localization signal (NLS), except DYRK3. Different than others, DYRK1A has one poly-histidine stretch (HIS), and a serine/threonine rich region (S/T). The Class II members, DYRK2, DYRK3 and DYRK4 have a N-terminal auto-phosphorylation accessory region (NAPA). Adapted from Singh & Lauth, 2017. Emerging roles of DYRK kinases in embryogenesis and Hedgehog pathway control, Journal of Developmental Biology, 5, 13.

Although functions of these domains are not fully characterized, distinct motifs had led to clues about their different possible functions. For instance, the PEST domain normally acts as a signal for rapid degradation, which needs to be tested for DYRK1A and DYRK1B. The HIS and S/T-rich region found only in DYRK1A promotes DYRK1A localization to nuclear speckles where they regulate splicing processes. Deletion of

DYRK1A have been implicated in mental retardation and primary microcephaly, which is supported *Drosophilia* and mice models of DYRK1A (O'Roak et al., 2012; Bon et al., 2011).

The class II of DYRKs autophosphorylate an essential tyrosine residue in the activation loop that enables phosphorylation of their substrates on serine and threonine residues. Phosphorylation of this activation loop happens intramolecularly during protein synthesis, and it is required for the kinase activity of class II DYRKs. The conserved NAPA domain is identified in DYRK2 via bioinformatic and mutational analysis, suggesting a chaperon like function which enables autophosphorylation of activation loop tyrosine, which at the end converting the class II DYRKs into transient intramolecular kinases (Singh & Lauth, 2017).

DYRKs mediate their functions during protein stability, cell proliferation, and differentiation via phosphorylating a wide range of substrates. The conserved sequence for the activation loop tyrosine is identified as YXY in vivo (Aranda et al., 2011), and phosphorylation leads to the full kinase activity. For the full activation, phosphorylation of the second Tyrosine residue is required, which gives the name of Dual specificity tyrosine regulated kinases. Current knowledge on the consensus sequence for the target protein phosphorylation includes Serine and Threonine residues followed by Proline in the position +1. Moreover, it is generally preferred to have an Arginine residue at the position -2 or -3 relative to Ser/Thr (RXXS/TP or RPXS/TP) (Singh & Lauth, 2017).

There are studies that revealed regulatory functions for DYRK family members during Hedgehog signaling and thereby linked them to embryonic brain development. Until now, DYRK1A, DYRK1B and DYRK2 have been determined as upstream and downstream regulators of Hedgehog signaling pathway via their activity on GLI transcription (Lauth et al., 2010; Mao et al., 2002; Varjosalo et al., 2008). DYRK1A was shown to positively regulate the Gli1 transcription activity (Mao et al., 2002). Differently, DYRK1B was shown to regulate Hh signaling negatively. In the context of the pancreatic cancer, overexpression of DYRK1B inhibits, and knockdown increases the Hh signaling pathway activity (Lauth et al., 2010; Singh & Lauth, 2017). The mechanisms by which DYRK1 family kinases regulate Hh signaling pathway is still not fully understood. For

the DYRK2, it is shown that both mammalian and Drosophila DYRK2 negatively regulates Hh signaling in part via phosphorylation and degredation of GLI2 (Varjosalo et al., 2008).

2.2 DYRK3

DYRK3 belongs to the class II dual specificity tyrosine phosphorylation-regulated kinases. Together with DYRK4, it is the least studied member of the DYRK kinase family. Importantly, DYRK3 defects were shown to promote hepatocellular carcinoma (Ma et al., 2019) and glioblastoma (Kyeongmin Kim et al., 2021). Additionally, DYRK3 was shown to be required for the replication of influenza virus (Bakre et al., 2013). As for its cellular functions, DYRK3 is shown to be important for liquid-liquid phase separation for the many membraneless organelles during mitosis in the cell including the centriolar satellites (PCM1) (Rai et al., 2018). DYRK3 couples stress granule condensation in the mechanism of mTORC1 signaling (Wippich et al., 2013). DYRK3 has also roles in the cytoskeletal organization, and axonemal and dendritic branching (Slepak et al., 2012).

To sum up, studies to date have characterized DYRK3 as an important regulator of mTORC signaling, phase transitions and vesicular trafficking. Its disease links suggest that DYRK3 might be involved in other cellular processes. Given the upregulation of DYRK3 in differentiating cultures of multiciliated epithelia, their regulatory roles during centriolar satellites biogenesis and the functions of other DYRK family members at the primary cilia, I hypothesized that DYRK3 might be a new regulator of ciligonesis. To test this and to elucidate DYRK3 functions during ciliogenesis, I used proteomics and cell biology approaches and dissected its regulatory roles at the cilia and satellites.

2.3 Results

2.3.1 Identification of DYRK3 interaction partners by mass spectrophotometry with an unbiased Bio-ID proximity labeling approach

To define the cellular interactors of DYRK3 in an unbiased way, I used the BioID-based proximity labelling approach to generate the in vivo proximity interactome. BioID approach is superior to traditional approaches in its ability to probe weak, transient and insoluble interactions and is thus it is the ideal method for identification of weak and transient DYRK3 interactors, in particular the substrates. In addition to wild-type DYRK3, I also identified the proximity interactome of kinase dead DYRK3 that might have a different interactome. Briefly, I expressed Flag-BirA-DYRK3 wild-type (WT), Flag-BirA-DYRK3 kinase-dead (KD), and Flag-BirA (Empty, E) in human embryonic kidney (HEK293T) cells, which are ideal for biochemistry experiments due to their high transfection efficiency and proliferative capacity. Moreover, this cell line was extensively used for BioID studies previously, which will give us a proxy for comparative analysis of DYRK3 proximity interactors with published BioID datasets for centriolar satellites, primary cilium and centrosome.

The experimental flow for the BioID experiment is shown in the Fig. 9A. First, I generated FLAG-BirA* fusions of DYRK3 and DYRK3 KD by performing Gateway reactions between pENTR-DYRK3 WT and KD into pDEST-FLAG-BirA* plasmids. Following verification of successful cloning by diagnostic digests, HEK293T cells were transfected with these plasmids and expression of fusion proteins and their ability to induce biotinylation was validated by western blot analysis with Flag and Streptavidin antibodies (Fig. 9B). In parallel to western blotting, I performed immunofluorescence analysis to validate localized biotinylation by the BirA*-fusions. To this end, transfected cells were incubated with vehicle control and biotin were stained for PCM1, Streptavidin and Flag. In agreement with published results, DYRK3 overexpression induced dissolution of satellites while DYRK3 KD did not (Rai et al., 2018) (Fig. 9C).

For the MS analysis, 5 x 15 cm HEK293T cells were transfected with Flag-BirA-DYRK3 WT, Flag-BirA-DYRK3 KD, and Flag-BirA (negative control). 24 h post-transfection, cells were incubated with 50 µm biotin for 18 h. Following biotin induction, cells were lysed under denaturing conditions and biotinylated proteins were pulled down using streptavidin agarose beads. Successful pulldown of biotinylated proteins was confirmed by immunoblotting with streptavidin that recognizes biotinylated proteins and FLAG antibody that recognizes the fusion protein (Fig. 9B). FLAG antibody detected FLAG-BirA* (about 35 kDA) and FLAG-BirA*-DYRK3 (about 110 kDa) at the expected sizes.

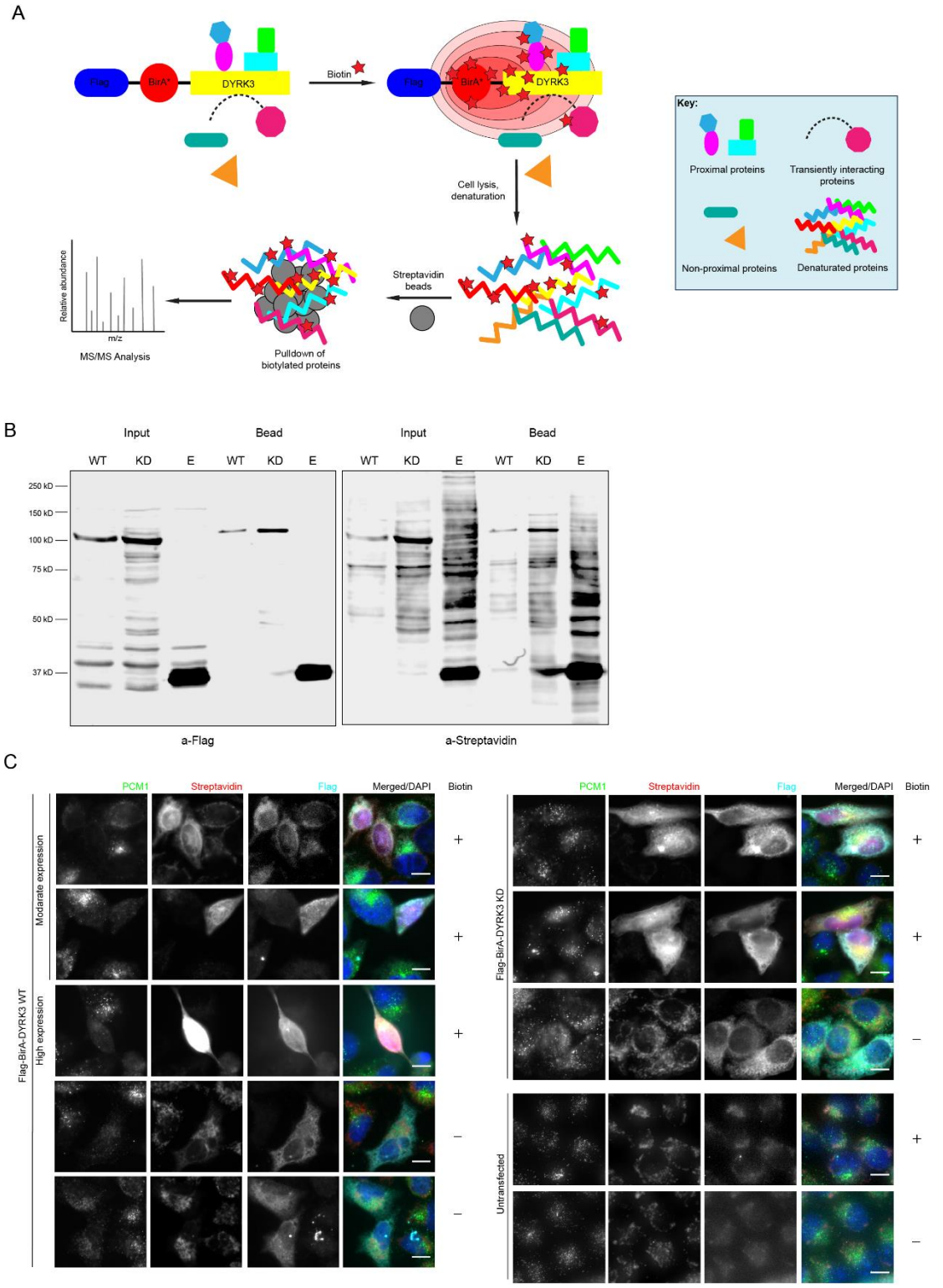

Figure 9: BioID proximity labelling of BirA-DYRK3, and confirmation of constructs. Workflow of BioID proximity labelling protocol. DYRK3 wild type or kinase dead constructs were used as bait protein fused with BirA enzyme. HEK293T cells

were transfected transiently with N-Flag-BirA (Empty, E), Flag-BirA-DYRK3 wild type (WT), and Flag-BirA-DYRK3 kinase dead (KD) constructs.

A. 50 μM biotin was added to cells for 18 hours as the substrate, which labels interactor proteins of DYRK3 either physically or transiently. After cell lysis, streptavidin pulldown was applied with streptavidin agarose beads, and interactor proteins were detected and analysed by MS analysis.

B. Biotinylated proteins from HEK293T lysates were captured with streptavidin agarose beads, resolved on SDS-PAGE gel and immunoblotted with streptavidin dye and flag antibodies.

C. Expression of constructs were confirmed by immunofluorescence analysis of cells stained for streptavidin, FLAG and the centriolar satellite marker PCM1. Untransfected cells were also shown as control.

2.3.2 High confidence proximity map of DYRK3 and DYRK3 KD mutant

To define the high confidence interactors of DYRK3 and its KD mutant, I performed label-free quantitative proteomics. Biotinylated proteins captured from large scale experiments were analysed at the Koc University Proteomics Facility. For the MS analysis, two biological replicates of Flag-BirA-DYRK3 WT, two biological replicates of Flag-BirA-DYRK3 KD, and two biological replicates of Flag-BirA were used. I identified the high-confidence proximity interactome of DYRK3 using Normalized Spectral Abundance Factor (NSAF) analysis removing the low-confidence interactors. First, I calculated NSAF values of every protein in the output list of MS analysis, and divided them into NSAF values of control spectral counts. Second, I determined the proteins having normalized NSAF values bigger than 1.0, which were 450 of them for WT and 483 of them for KD. Third, I feed these proteins into The Contaminant Repository for Affinity Purification (CRAPome) (Mellacheruvu et al., 2013) database to filter out the possible common mass spectrophotometry contaminants. From the CRAPome list, I determined the proteins identified in less than 200 experiments out of 716 in the database. After filtering, this threshold yielded 254 proteins as high-confidence interactors for wild type (Fig. 10A) and 282 for kinase dead construct (Fig. 10B).

I analysed the network clusters using Cytoscape software (Shannon et al., 2003). First, I uploaded the high proximal interactors to STRING database to map the interactions between the interactor proteins (Szklarczyk et al., 2019). Then, I generated functional clusters using ClusterONE (Nepusz et al., 2012) plug in of Cytoscape, comparing the retrieved clusters also with PANTHER Gene Ontology (Mi et al., 2019), EnrichR (Chen et al., 2013), BioGRID (Oughtred et al., 2021), and DAVID (Huang et al., 2009) and data mining using UniProt (The UniProt Consortium, 2021) databases.

As shown in the Fig. 2, main clusters identified as a result of the above-mentioned analysis were nuclear compartments, vesicular trafficking, centriolar satellites, DNA binding/repair, RNA binding/splicing, ribosome biogenesis, and protein ubiquitination for wild type, and additionally nuclear import and cell-cell junctions were enriched for DYRK3 KD. We noted that a group of proteins implicated developmental and proliferation were among high confidence interactors but they were not part of the major GO clusters identified by our analysis.

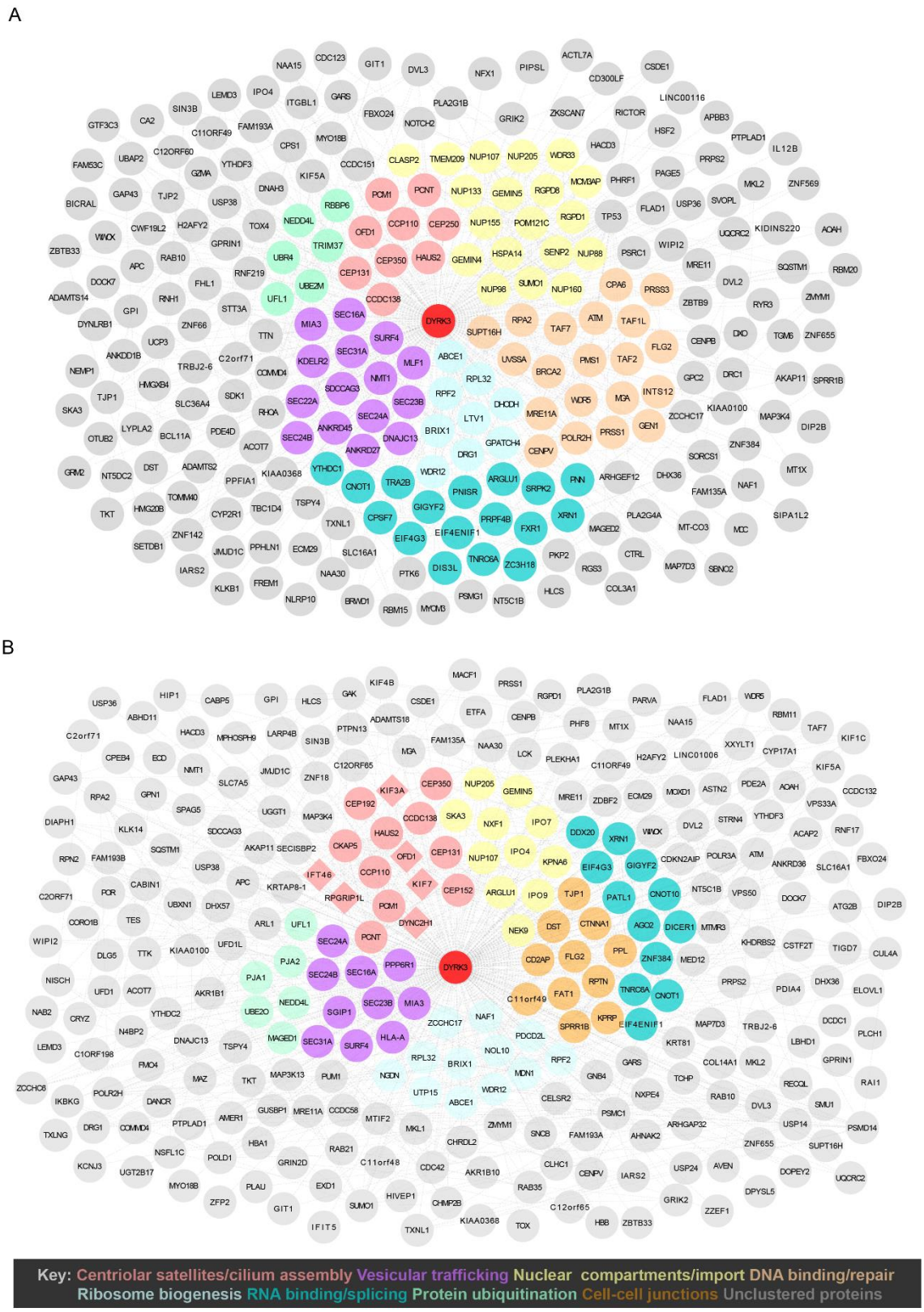

Figure 10: High confidence proximity map of DYRK3 and DYRK3 KD mutant.

A. High confidence proximity map of DYRK3. Interactor network map shows DYRK3 WT BioID interactors after NSAF analysis (> 1.0), and CRAPome filtering. 254 proteins were determined as high confidence interactors of DYRK3. **B.** High confidence proximity map of DYRK3 KD mutant. Interactor network map shows DYRK3 kinase dead BioID interactors after NSAF analysis (> 1.0), and CRAPome filtering. 282 proteins were determined as high confidence interactors of DYRK3 KD mutant.

Key shows the colour code of functional clusters as Centriolar satellites/cilium assembly (♦) (pink), vesicular trafficking (purple), DNA binding/repair (light orange), nuclear compartments/import (yellow), ribosome biogenesis (light blue), RNA binding/splicing (blue), protein ubiquitination (green), cell-cell junctions (orange), und unclustered proteins (light grey).

2.3.3 DYRK3 wild type interaction partners are components of different cellular compartments including centriolar satellites

DYRK3 high confidence proximity map consisted of 254 proteins. 19 of these proteins were implicated in nuclear functions including the ones related to Protein Sumoylation, and PML-body and P-body. This category included the following proteins: CLASP2, GEMIN4, GEMIN5, HSPA14, MCM3AP, NUP107, NUP133, NUP155, NUP160, NUP205, NUP88, NUP98, POM121C, RGPD1, RGPD8, SENP2, SUMO1, TMEM209, WDR33.

The second enriched cluster included DNA binding and repair proteins: WDR5, UVSSA, TAF7, TAF2, TAF1L, SUPT16H, RPA2, PRSS3, PRSS1, POLR2H, PMS1, MRE11A, MGA, INTS12, GEN1, FLG2, CPA6, CENPV, BRCA2 and ATM.

The third enriched cluster included vesicular trafficking proteins, SURF4, SEC31A, SEC24B, SEC24A, SEC23B, SEC22A, SEC16A, MIA3, KDELR2 and ANKRD45.

The fourth enriched cluster included satellite/ centrosome proteins. implicated in cilium assembly and microtubule binding processes. This group included PCNT, PCM1, OFD1, HAUS2, CEP350, CEP250, CEP131, CCP110 and CCDC138.

The fifth enriched cluster included RNA binding and splicing proteins, ZC3H18, YTHDC1, XRN1, TRA2B, TNRC6A, SRPK2, PRPF4B, PNN, PNISR, GIGYF2, FXR1, EIF4G3, EIF4ENIF1, DIS3L, CPSF7 and CNOT1.

The sixth cluster included ribosome biogenesis proteins WDR12, RPL32, RPF2, LTV1, GPATCH4, DRG1, DHODH and BRIX1.

The seventh enriched cluster included proteins implicated in protein ubiquitination, which are UFL1, UBR4, UBE2M, TRIM37, RBBP6 and NEDD4L (Fig. 11A).

To define new DYRK3 functions and regulatory mechanisms, I performed Gene Ontology (GO) enrichment analysis of the high confidence interactors of DYRK3 wild type BioID using EnrichR (Chen et al., 2013). The significant ($p < 0.005$) enriched GO terms for cellular component were nuclear body, PML body, transcription factor TFIID complex, nucleolus, polysome in a nuclear concept, and COPII vesicle coat, endoplasmic reticulum exit site in a vesicular trafficking concept, and centrosome, centriole, and centriolar satellites in a cytoskeleton concept. These enrichments were consistent with the previous research, and also revealed new possible compartmentalization. The significant ($p < 0.05$) enriched biological processes revealed new possible functions as regulation of gene silencing by miRNA, protein sumoylation, regulation of translation, nuclear import, protein import, mRNA transport, viral life cycle, ribosome biogenesis, DNA repair, and cilium assembly. The significant ($p < 0.005$) enriched molecular functions were determined as binding of RNA, microtubule plus-end, nuclear localization sequence, ribosome, protease, DNA, gamma-tubulin, and mRNA, and activity of transcription factor and protein transporter. Importantly, the proximity interactions of DYRK3 included previously published interactors including centriolar satellite, vesicular trafficking, PML bodies, validating our approach. The proximity relationship of DYRK3 is in agreement with our hypothesis that it functions during cilium biogenesis and also suggests mechanisms by which DYRK3 regulates ciliogenesis (Fig 11B).

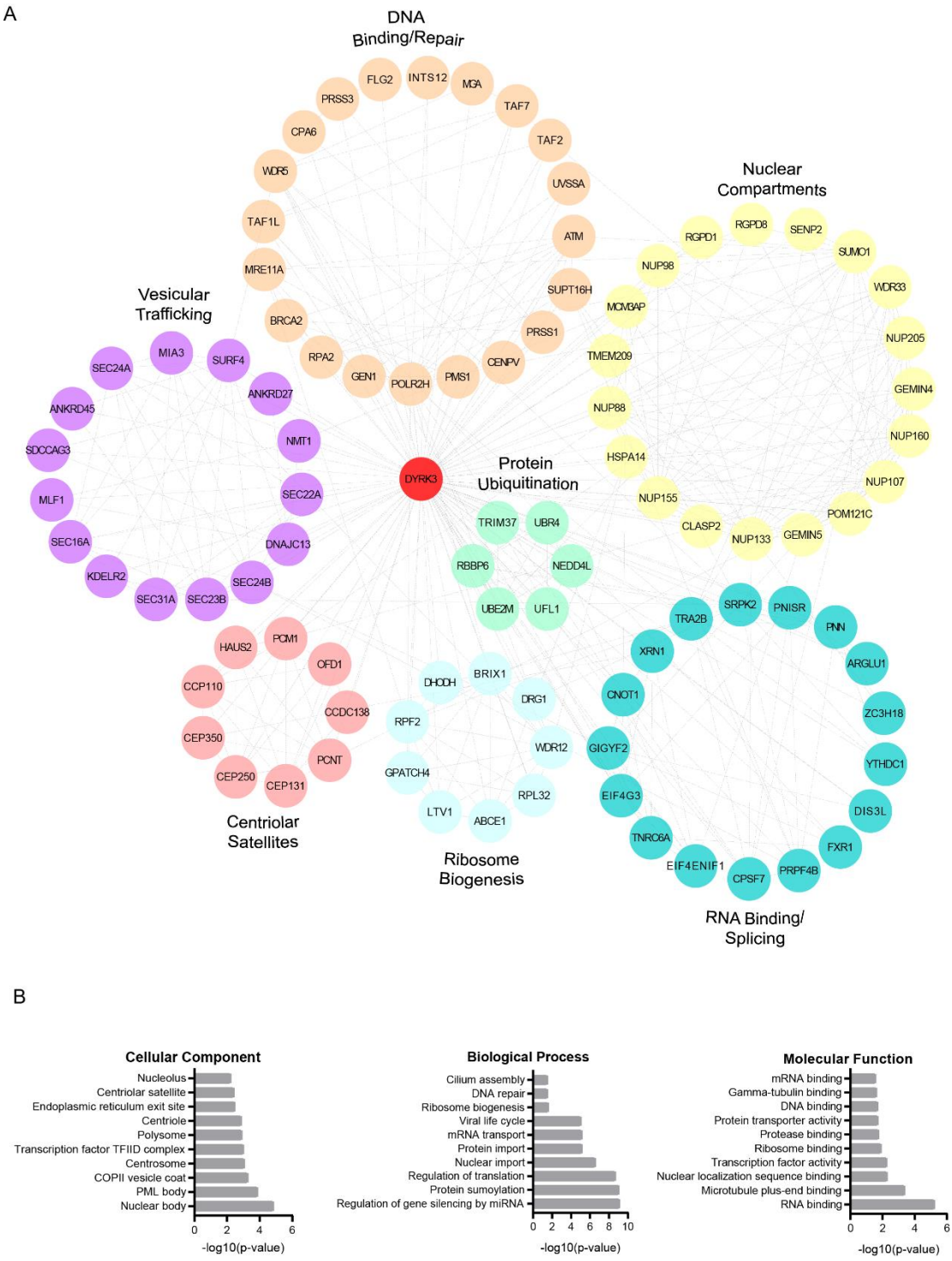

Figure 11: Enriched functional clusters of DYRK3.

A. High confidence proximity interactors of DYRK3 were determined using NSAF analysis. The proximal interactors were ranked by their fold change in DYRK3 WT dataset relative to control. Remaining 254 proteins after CRAPome were feed into STRING database to determine interactions between interactors. Cytoscape was used to visualize interactions of high confidence interactor proteins, and

functional clusters were determined with ClusterONE plug-in. Seven functional clusters were enriched in the interactome, including centriolar satellites (pink), vesicular trafficking (purple), nuclear compartments (yellow), DNA binding/repair (light orange), ribosome biogenesis (light blue), RNA binding/splicing (blue), and protein ubiquitination (green). Unclustered proteins were not shown in the enriched network.

B. GO enrichment analysis of DYRK3 proximity interactors based on their cellular component, biological process, and molecular function. X-axis shows the minus log-transformed p-values (Fisher's exact test) of GO terms.

2.3.4 Kinase dead version of DYRK3 have interaction partners in different cellular compartments also including centriolar satellites

DYRK3 KD high confidence proximity map consisted of 282 proteins. From these proteins, 11 of them are implicated in nuclear import proteins GEMIN5, ARGLU1, KPNA6, NXF1, IPO7, NUP205, NUP107, SKA3, IPO4, NEK9 and IPO9.

The second enriched cluster included satellite/ centrosome proteins implicated in cilium assembly and microtubule binding processes. This group included KIF7, CCP110, PCM1, KIF3A, HAUS2, DYNC2H1, CEP131, OFD1, PCNT, IFT46 and CCDC138.

The third enriched cluster included vesicular trafficking proteins SEC16A, SEC24A, HLA-A, SEC23B, SEC31A. MIA3, HACD3, SEC24B, PPP6R1, SGIP1 and SURF4.

The forth enriched cluster included RNA binding and splicing proteins AGO2, CNOT1, CNOT10, DDX20, DICER1, EIF4ENIF1, EIF4G3, GIGYF2, PATL1, TNRC6A, XRN1 and ZNF384.

The fifth enriched cluster included ribosome biogenesis proteins ABCE1, BRIX1, MDN1, NAF1, NGDN, NOL10, PDCD2L, RPF2, RPL32, UTP15, WDR12 and ZCCHC17.

The sixth enriched cluster included proteins implicated in protein ubiquitination, which are MAGED1, NEDD4L, PJA1, PJA2, UBE2O and UFL1.

The seventh enriched cluster included cell-cell junction proteins C11orf49, CD2AP, CTNNA1, DST, FAT1, FLG2, KPRP, PPL, RPTN, SPRR1B and TJP1 (Fig. 12A).

To define DYRK3 functions and regulatory mechanisms for kinase dead, I performed Gene Ontology (GO) enrichment analysis of the high confidence interactors of DYRK3 kinase dead BioID using EnrichR (Chen et al., 2013). The significant ($p < 0.05$) enriched GO terms for cellular component were P body, RISC complex, and nuclear membrane in a nuclear concept, and COPII vesicle coat in a vesicular trafficking concept, and microtubule cytoskeleton, intermediated filament cytoskeleton, mitotic spindle, cilium, and deuterosome in a cytoskeleton concept. These enrichments revealed possible compartmentalization when the protein loses its kinase activity. The significant ($p < 0.0005$) enriched biological processes revealed new possible functions as regulation of mRNA processes, regulation of cell cycle g2/M phase transition, ciliary docking, COPII-coated vesicle cargo loading, regulation of translation, endomembrane system organization, protein localization to MTOC, protein import into nucleus, cilium assembly, and wound healing. The significant ($p < 0.05$) enriched molecular functions were determined as binding of RNA, microtubule, cadherin, mRNA, protein phosphatase, and ribosome, and activity of motor, deubiquitinase, retinal dehydrogenase, and endonuclease (Fig. 12B). We highlighted that DYRK3 KD interactome contained more proteins implicated in ciliogenesis, which might have important implications for its functions at the primary cilium.

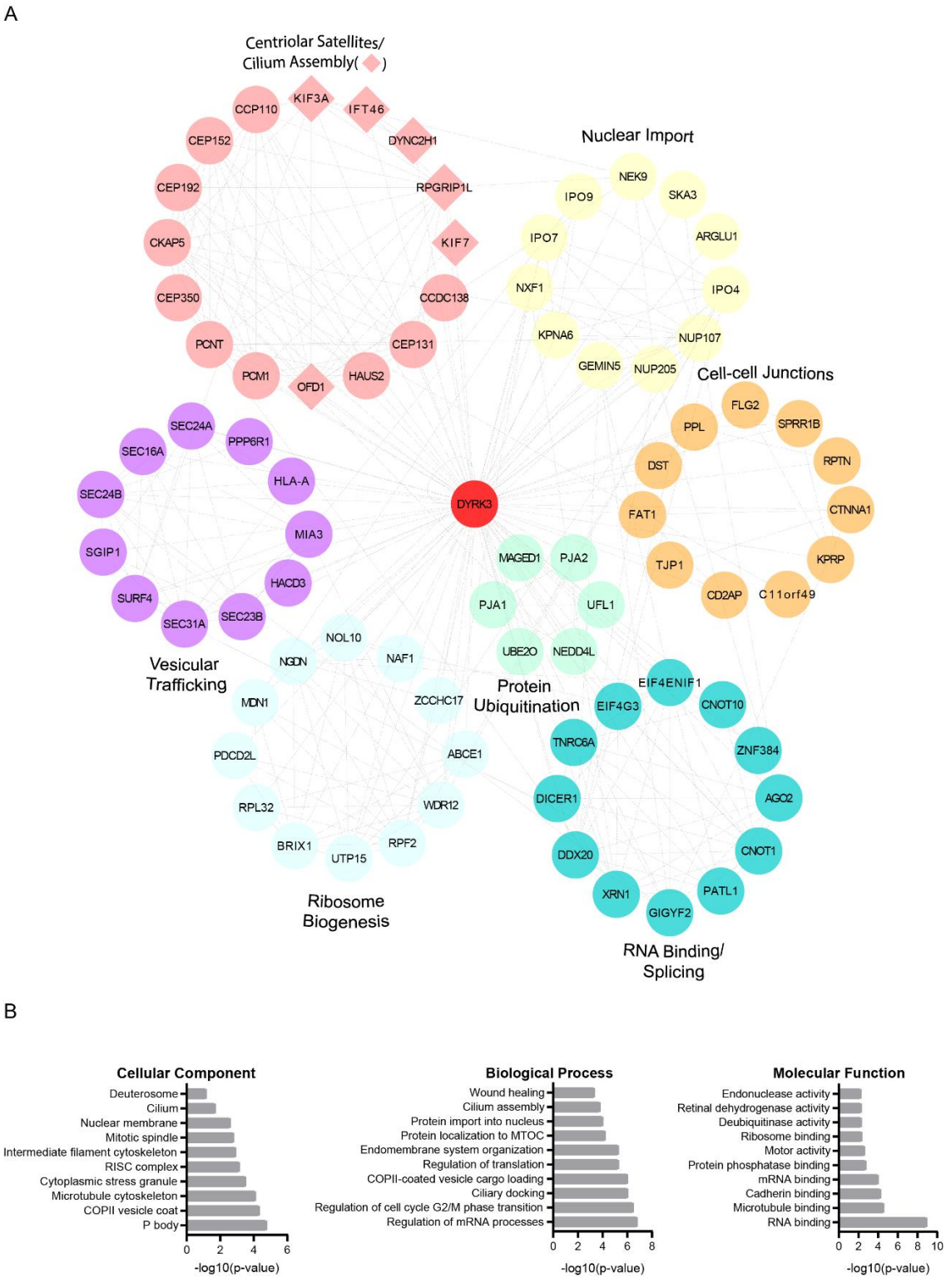

Figure 12: Enriched functional clusters of DYRK3 kinase mutant.

A. High confidence proximity interactors of DYRK3 KD are determined using NSAF analysis. The proximal interactors were ranked by their fold change in the DYRK3 KD relative to control. Remaining 282 proteins after CRAPome were

feed into STRING database to determine interactions between interactors. Cytoscape was used to visualize interactions of high confidence interactor proteins, and functional clusters are determined with ClusterONE. Seven functional clusters were enriched in the interactome, including centriolar satellites/ cilium assembly (pink), vesicular trafficking (purple), nuclear import (yellow), ribosome biogenesis (light blue), RNA binding/splicing (blue), protein ubiquitination (green), and cell-cell junctions (orange). Unclustered proteins were not shown in the enriched network.

B. GO enrichment analysis of DYRK3 kinase dead proximity interactors based on their cellular component, biological process, and molecular function. X-axis shows the minus log-transformed p-values (Fisher's exact test) of GO terms.

2.3.5 Comparison of wild type and kinase dead version of DYRK3 proximal interactors

Bio-ID proximal interactors of wild type and kinase dead retrieved 118 common protein interactors. They included different enriched clusters. The proteins identified in the only wild type DYRK3 were 136 high confidence interactors, and the proteins identified in the only kinase dead DYRK3 were 164 high confidence interactors (Fig. 13A). Functional clusters retrieved from ClusterONE were shown in colour codes as centriolar satellites/ cilium assembly (pink), vesicular trafficking (purple), DNA binding/repair (light orange), nuclear compartments/import (yellow), ribosome biogenesis (light blue), RNA binding/splicing (blue), protein ubiquitination (green), cell-cell junctions (orange), and unclustered proteins (light grey).

The GO ontology analysis show that DYRK3 wild-type-specific proteins were enriched for nuclear compartments, while the ones specific for KD were for cytoskeletal processes (Fig. 13B). The functional significance as well as the molecular basis of this difference needs further investigation.

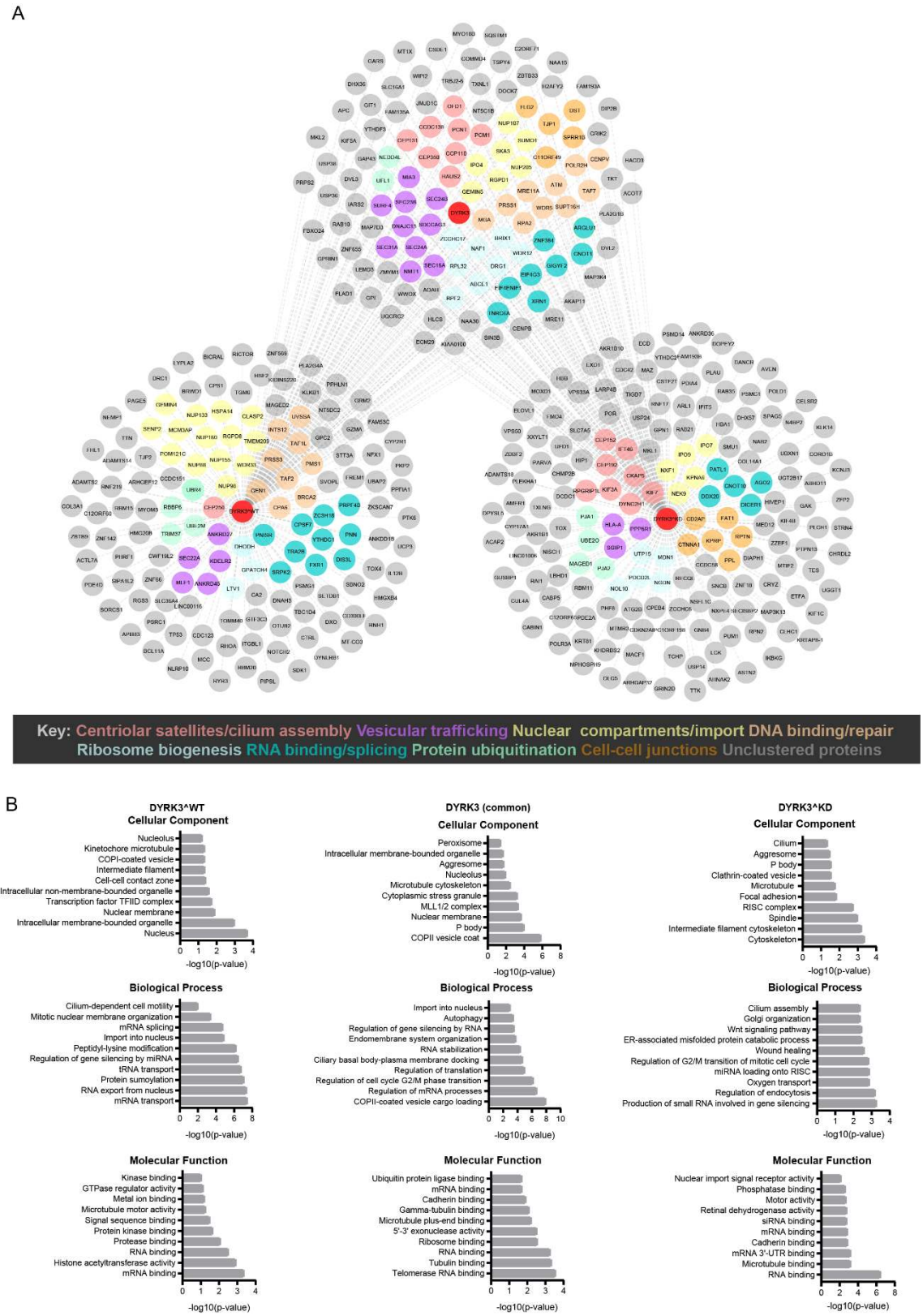

Figure 13: Comparison of wild type and kinase dead version of DYRK3 proximal interactors.

A. The comparison of high confidence interactors of DYRK3 and DYRK3 KD retrieves 118 common protein interactors. 136 proteins were determined only in wild type dataset, and 164 proteins were determined only in kinase dead dataset. Functional clusters retrieved from ClusterONE were shown in colour codes in the key as centriolar satellites/ cilium assembly (pink), vesicular trafficking (purple), DNA binding/repair (light orange), nuclear compartments/import (yellow), ribosome biogenesis (light blue), RNA binding/splicing (blue), protein ubiquitination (green), cell-cell junctions (orange), and unclustered proteins (light grey).

B. GO enrichment analysis of DYRK3 and DYRK3 KD high confidence interactors after comparison as only wild type, common, and only kinase dead. GO enrichment analysis were shown based on their cellular component, biological process, and molecular function. X-axis shows the minus log-transformed p-values (Fisher's exact test) of GO terms.

2.3.6 Identification of DYRK3 interaction partners reveals novel interactors comparing with the previous research

After identifying high confidence interactors of DYRK3, I compared the DYRK3 proximity maps generated from DYRK3 WT and KD Bio-ID with the SILAC-based quantitative proteomics data from overexpressed EGFP-DYRK3 cells with or without GSK-626616 data reported in the Rai et al., 2018 paper, and also in the Biological General Repository for Interaction (BioGRID) database (Oughtred et al., 2021). DYRK3 WT data shares 14 interactors with the EGFP data. These shared interactors were mainly enriched in vesicular trafficking components (Fig. 14A). When DYRK3 BioID WT and EGFP SILAC data was also compared with BioGRID database, the common protein for all three is the DYRK3. NEDDL4 was the common interactor for BioID WT and BioGRID database (Fig. 14B).

Next, I compared the interactor proteins in the list of BioID KD and EGFP SILAC GSK-626616. It retrieved 20 shared interactors, which were enriched in components of vesicular trafficking and nuclear compartments (Fig. 14C). When I compared these data

sets also with BioGRID, DYRK3 was the common interactor for all there, and NEDDL4 and SMU1 were the common interactors both in BioID KD and BioGRID data sets (Fig. 14D).

As shown in the Fig. 14E, there are 118 common interactors in WT and KD BioID. 136 proteins were identified only in WT, and 164 proteins were identified only in KD. The different interactors and their corresponding GO enrichment analysis were reported in the Fig. 13. The comparison of the four datasets (BioID WT and KD, EGFP SILAC and GSK-626616) was shown in the Fig. 14F. As a result, we identify previously undescribed DYRK3 interactors with an unbiased approach in two different conditions.

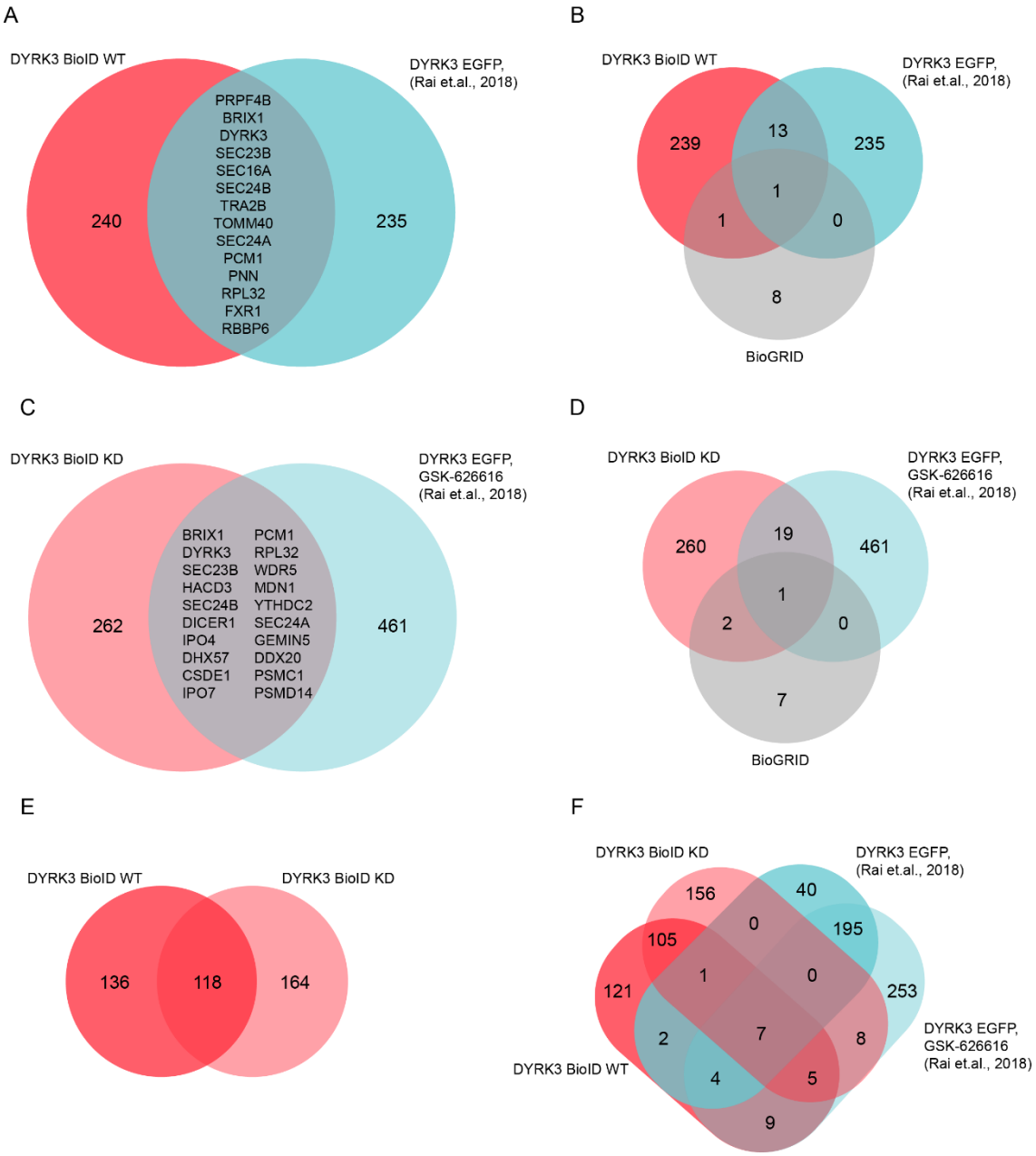

Figure 14: Determination of DYRK3 interaction partners identified in the published research.

A. Comparison of DYRK3 wild type proximity interactome with the published EGFP DYRK3 data retrieved 14 overlapping, and 240 distinct interactors.

B. Comparison of DYRK3 wild type proximity interactome, EGFP DYRK3 data, and BioGRID database for the published interactors.

C. Comparison of DYRK3 kinase dead proximity interactome with the published EGFP DYRK3 treated with GSK-626616 dataset retrieved 20 overlapping, and 262 distinct interactors.

D. Comparison of DYRK3 kinase dead proximity interactome, EGFP DYRK3 treated with GSK-626616 dataset, and BioGRID database for the other published interactors.

E. Venn diagram shows comparison of DYRK3 wild type proximity interactome with DYRK3 kinase dead proximity interactome.

F. The comparison of the four datasets: DYRK3 BioID wild type and kinase dead, EGFP DYRK3 and treated with GSK-626616.

2.3.7 DYRK3 physically interacts with the core centriolar satellite components

Proximity relationship means that the bait protein is within 10-20 nm proximity of the identified preys, which might be direct or indirect interactors and do not necessarily mean physical interactors. To test whether proximity relationships are reflected as physical interactors, I performed immunoprecipitation (IP) experiments. As baits to be tested in IP experiments, I focused on the scaffolding protein for centriolar sateliltes (PCM1) and two core satellite proteins CEP131 and OFD1. I chose these proteins due to their published roles during primary cilium assembly and function (Hall et al., 2013; Wilkinson et al., 2009; Ferrante et al., 2006; Romio et al., 2004). To validate the physical interaction between DYRK3 and PCM1, I performed streptavidin pulldowns with HEK293T cells overexpressing Flag-BirA (E) as control, and Flag-BirA-DYRK3 wild type and kinase dead constructs, and immunoblotting against PCM1 antibody after confirming the successful pulldown as shown in Fig. 9B. From these Bio-ID streptavidin pulldown experiments, I validated the PCM1 interaction of DYRK3 both for wild type and kinase dead comparing with the empty control (Fig. 15A).

After confirming interaction with the scaffolding centriolar satellite protein, I wanted to validate DYRK3 interaction with CEP131 and OFD1, which are core components of centriolar satellite having function in ciliogenesis. I validated CEP131 and OFD1 interactions of DYRK3 by immunoblotting BioID streptavidin pulldown samples against CEP131 and OFD1 antibodies (Fig. 15A). These interactions might be an indication for possible function of DYRK3 in ciliogenesis.

Next, I wonder whether DYRK3 physically interacts with centriolar satellites to further validate the datasets. For the confirmation, I performed co-immunoprecipitation (Co-IP) experiments from HEK293T cells either asynchronized or synchronized in mitosis. The reason why we include mitotic synchronized cells is to check whether PCM1 interaction is affected during mitosis when DYRK3 activity and level increases (Rai et al., 2018). After co-expression of EGFP-PCM1 with Flag-BirA (E) as control, and Flag-BirA-DYRK3 wild type or kinase dead constructs, pulldowns were performed with flag beads. The successful flag pulldown was confirmed by immunoblotting against FLAG antibody. Immunoblotting against PCM1 and GFP antibodies validated the physical interaction of PCM1 with DYRK3 (Fig. 15B).

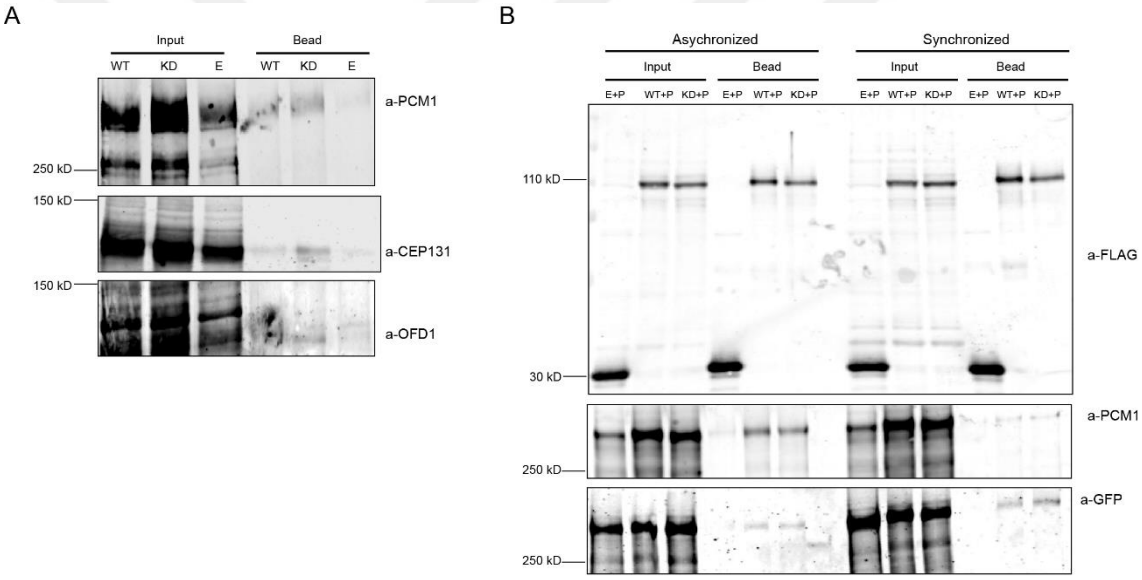

2.3.8 Physical interaction of DYRK3 with core satellite components were validated via IP experiments.

A. DYRK3 interacts with centriolar satellite proteins having functions in ciliogenesis, PCM1, CEP131, and OFD1. HEK293T cells were transiently transfected with Flag-BirA (E) as control, and Flag-BirA-DYRK3 wild type (WT) and kinase dead (KD). The cells were incubated with 50 μM biotin for 18 hours, and biotinylated proteins were pulled down with streptavidin beads. Input and pulled down samples were immunoblotted antibodies against PCM1, CEP131 and OFD1.

B. DYRK3 physically interacts with PCM1 in asynchronous and mitotic conditions. EGFP-PCM1 (P) was co-expressed with Flag-BirA (E) as control, and Flag-BirA-

DYRK3 wild type (WT) and kinase dead (KD) in HEK293T cells. After 24 hours transfection, cells were treated with either DMSO for asynchronized cells, or 10 μM STLC for 20 hours for cells synchronized at mitosis. The cells were lysed and pulled down with flag beads. Input and elutes samples were immunoblotted with antibodies against FLAG, PCM1 and GFP.

2.3.9 DYRK3 has a role on ciliogenesis as a novel mechanism

Together with the DYRK3 proximity interaction map, there are three lines of evidence that supports functions for DYRK3 during cilia biogenesis. First, DYRK3 expression increases about 20 fold (4.35 = $\log^2$ fold change) at ALI-4 during centriole amplification and initiation of motile cilia assembly, and about 12 fold (3.57 = $\log^2$ fold change) at ALI-12 during motile cilia assembly (Hoh et al., 2012). Upregulation of DYRK3 expression in differentiating MTEC cells suggest that it is a regulator of centriole amplification and/or motile cilia assembly. Second, DYRK3 was reported as an upstream kinase that is required for mitotic dissolution of satellites (Rai et al., 2018). Given the important regulatory functions of centriolar satellites during primary cilium and motile cilia assembly, this finding suggests that DYRK3 might regulate these processes via centriolar satellites. Finally, DYRK3 WT and KD proximity interactome consisted key regulators of cilium biogenesis including PCM1, CEP131, OFD1, KIF7, IFT42, CEP152. Using immunoprecipitation studies, I validated that the proximity relationship of DYRK3 with PCM1 and CEP131 is reflected at the physical level. Collectively, these results motivated us to test the functions of DYRK3 during primary cilium assembly.

For ciliogenesis experiments, I used human retinal pigment epithelium (RPE1) cells that form primary cilium upon serum starvation and thereby widely used for primary cilium research. To test the putative functions of DYRK3 during primary cilium biogenesis, I treated confluent RPE1 cells with vehicle control and DYRK3 inhibitor and quantified the percentage of ciliation upon serum starvation. Experimental workflow is shown in Fig. 16A. First, RPE1 cells were seeded to coverslips and grown in complete medium until they reach confluency. After they became fully confluent, complete medium was replaced by serum starvation medium without FBS to induce ciliogenesis. At the time of

medium change, I treated cells with DMSO as control or 1 μM GSK-626616, which is a confirmed DYRK3 inhibitor (Wippich et al., 2013; Rai et al., 2018). Following 24 h of incubation, cells were fixed with cold methanol for immunofluorescent staining (Fig. 16A). The fixed cells were stained with antibodies against PCM1 that marks centriolar satellites, glutamylated tubulin (GT335) and the small GTPase ARL13B that marks primary cilium. As shown in Fig. 16B, DYRK3-inhibited cells had longer cilia with architectural defects as compared to cilia that formed in control cells (Fig. 16B). Like DYRK3, DYRK2 depletion was previously reported to result in increased cilium length via an AURKA-dependent mechanism (Yoshida et al., 2020). In addition to cilium length, I compared control and DYRK3-inhibited cells for their ciliation efficiency and for pericentrosomal clustering. DYRK3 inhibition resulted in a significant decrease in the percentage of ciliated cells relative to control cells ($p = 0.0008$) (Fig. 16C), and ciliated cells form longer cilium significantly ($p < 0.0001$) (Fig. 16D). Additionally, DYRK3 inhibition resulted in a significant decrease in PCM1 level on basal body ($p < 0.0001$) (Fig. 16E).

Finally, to assess the morphological changes of the cilium linked to DYRK3 inhibition, I performed Ultrastructure Expansion Microscopy (U-ExM) approach which allows to observe proteins in a nanoscale mapping at the centrosomes and cilia (Gambarotto et al., 2018; Le Guennec et al., 2020). As shown in Fig. 16F, cells were crosslinked in a polymer matrix which allows post-expansion immunostaining, and gels were stained with antibodies against polyglutamylated tubulin (GT335) and acetylated tubulin (AcTub) as cilium markers. Basal bodies and primary cilium structures were shown in the Fig. 16F, and the cilium length extension phenotype was apparent upon DYRK3 inhibition, further corroborating its functions during axonemal length regulation.

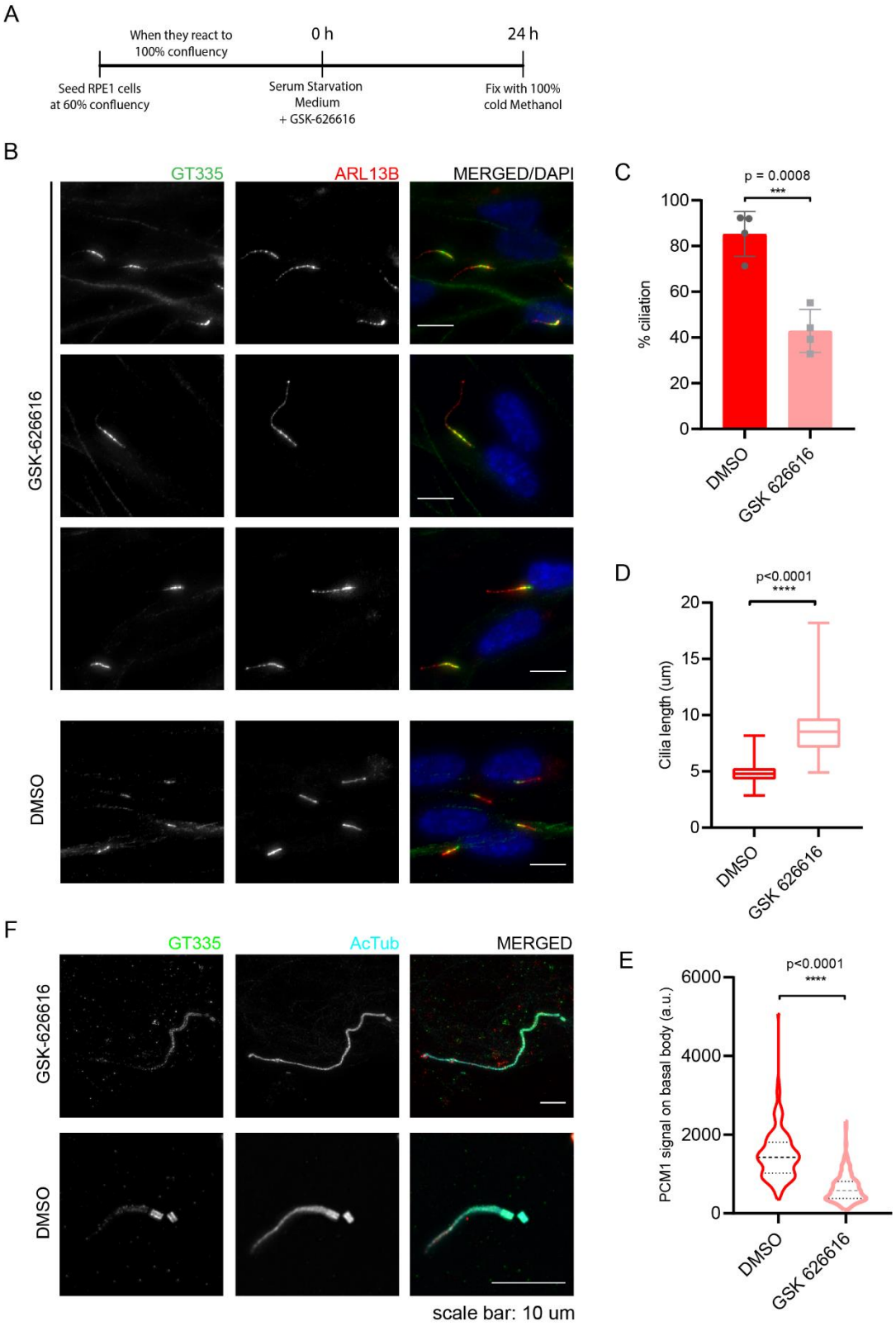

Figure 16: DYRK3 has a role in primary cilium assembly.

A. Experimental flow of cilium assembly upon DYRK3 inhibition.

B. RPE1 cells were seeded into 24-well coverslips with complete medium. When they became fully confluent, cells were treated with serum starvation medium without FBS containing DMSO or 1 µM GSK-626616 for 24 hours. Cells were fixed with cold methanol, and immunostained against antibodies polyglutamylated tubulin (GT335) and acetylated tubulin (AcTub) as cilium markers. DAPI was used to stain the DNA. Scale bar, 10 µm.

C. Quantification of percentage of cells that formed cilia upon DYRK3 inhibition. n > 100 cells per experiment. Data represents mean values of four experiment per condition +-SEM (*** $p = 0.0008$).

D. Quantification of cilia length (um) upon DYRK3 inhibition. n > 100 cells per experiment. Data represents mean values of two experiment per condition +-SEM (**** $p < 0.0001$).

E. Quantification of PCM1 signal on basal body (a.u.) upon DYRK3 inhibition. PCM1 signal was measured using ImageJ as centrosomal fluorescence intensity in a 3 μm^2 square area around the basal body using GT335 signal. n > 100 cells per experiment. Data represents mean values of two experiment per condition +-SEM (**** $p < 0.0001$).

F. High resolution representation of cilium length increase upon DYRK3 inhibition by U-ExM. RPE1 cells were seeded into 24-well coverslips with complete medium. When they became fully confluent, the cells were treated with serum starvation medium without FBS containing DMSO or 1 µM GSK-626616 for 24 hours. After expansion by U-ExM, cells were immunostained against antibodies polyglutamylated tubulin (GT335) and acetylated tubulin (AcTub) as cilium markers. Scale bar, 10 µm.

2.3.10 In vitro investigation of ciliogenesis role of DYRK3 in MTEC model system

Given that DYRK3 is transcriptionally upregulated during differentiation of in vitro MTEC cultures (Hoh et al., 2012), it is likely that DYRK3 is also required for motile cilium assembly. To test this, I assayed the phenotypic consequences of DYRK3 inhibition in MTEC cultures fixed at ALI-4 and ALI-12. ALI-4 is the stage where genes involved in the centriole duplication were shown to be enriched, and ALI-12 is the stage where genes involved in mature cilia assembly were shown to be enriched. ALI-8 is an intermediate stage, during when there is a heterogenous population including cells in centriole duplication, cilium assembly and mature cilia processes (Mahjoub et al., 2010).

To examine whether DYRK3 has a role in multi-ciliation, I used MTEC cultures as a primary cell culture method. I dissected trachea from mice, and seeded the isolated epithelial cells into filters to model air liquid interphase (ALI) in vitro. After filters became fully confluent, I changed to MTEC differentiation medium containing DMSO as control or treated with 1 μM GSK-626616 as DYRK3 inhibitor (Fig. 17A). Fresh medium was supplemented in every two days containing DMSO or 1 uM GSK-626616. At ALI-8, filters were fixed with cold methanol, and immunostained antibodies against acetylated tubulin (AcTub) as cilium marker, Centrin as centriole marker and ZO-1 as epithelial cell boundary marker indicating the differentiation (Fig. 17B).

In ALI-8, we observed a heterogenous population of cells in both conditions as expected. Although centrioles were homogenously distributed at the apical base of the cell in the controls, we observed a defective centriole docking phenotype upon DYRK3 inhibition. Additionally, their cilia rotations were angled and disruptive comparing with the control. Collectively, these results showed that DYRK3 might be required for centriole docking/splitting, motile cilia assembly and centriole amplification during differentiation of MTEC cultures.

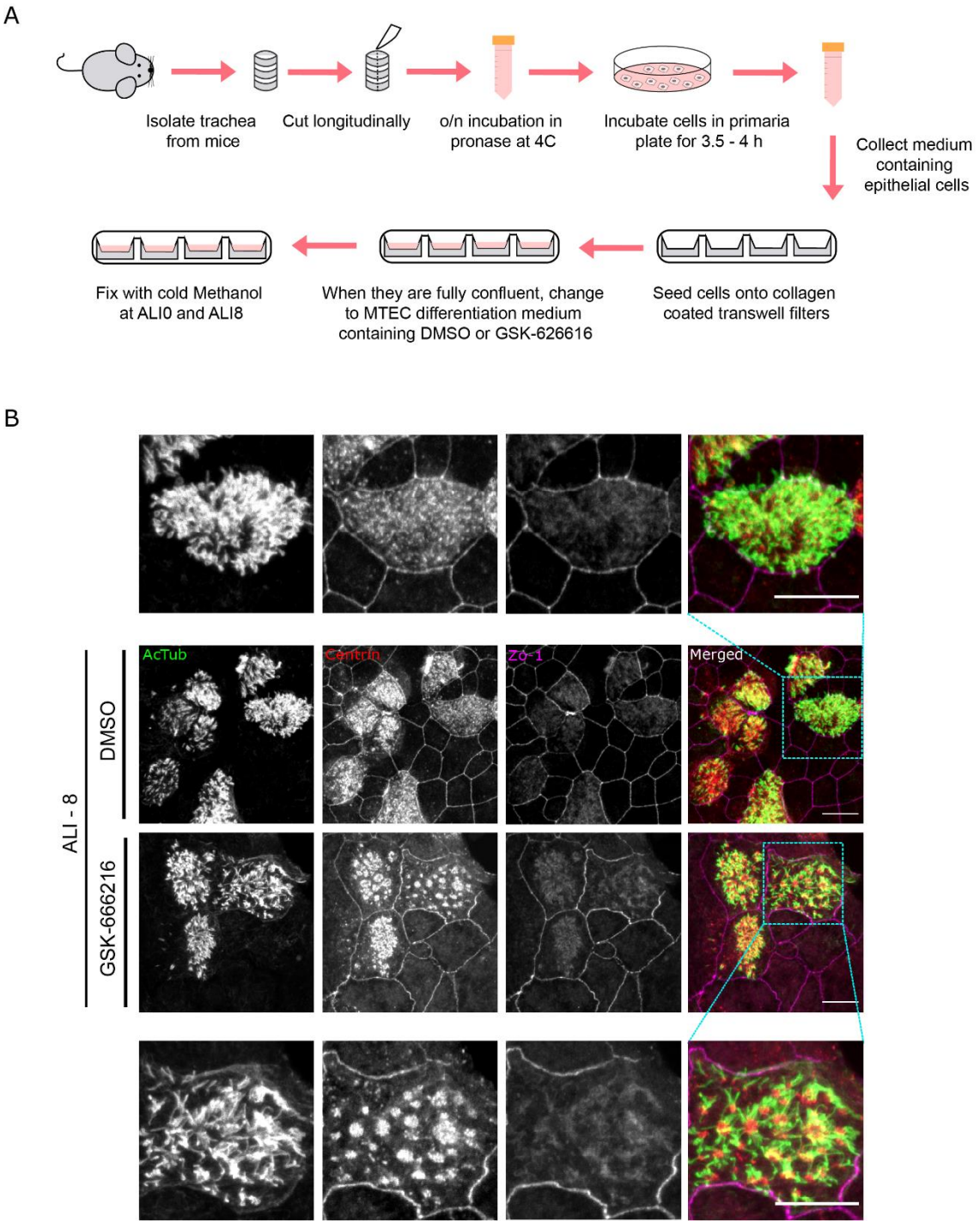

Figure 17: In vitro investigation of ciliogenesis role of DYRK3 in MTEC model system reveals possible function of DYRK3 in multi-ciliation.

A. Experimental representation of MTEC primary cell culture method. Trachea were isolated from wild type BALB/C mice, and cut longitudinally after external tissues were removed. Isolated trachea was incubated in 1.5 mg/ml pronase for overnight (o/n). In the following day, isolated cells were resuspended, and incubated in Primaria plate for 3.5-4 hours to adhere

fibroblasts while allowing epithelial cells remain in the solution. After collection of epithelial cells, 100.000 cells were seeded onto collagen coated Transwell inserts. The cells were allowed to grow for 2 days, and medium is changed every 2 days. After cells were become fully confluent, medium was changed to ALI media to induce differentiation. Cells were treated either with ALI media containing DMSO or GSK-626616, and fixed with cold methanol at the 8th day of the differentiation (ALI-8). Then, filters were immunostained antibodies against acetylated tubulin (AcTub), Centrin and ZO-1.

B. DYRK3 inhibition results in defective centriole docking and cilia phenotype. ALI-8 filters were immunostained antibodies against acetylated tubulin (AcTub), Centrin and ZO-1. 2-fold zoom-in images are shown at the above of DMSO, and at the below of GSK-626616 conditions. Confocal microscopy images are deconvolved. Scale bar, 10 μM.

2.4 Discussion

In this study, I generated the first in vivo proximity interaction map of DYRK3 and its kinase dead mutant and used functional assays to characterize DYRK3 as a new player of primary cilium biogenesis. In addition to uncovering a previously undescribed relationship between DYRK3 and primary cilium, its proximity map will provide an important resource for the field. Through interaction studies and functional assays, I validated the reliability of the DYRK3 proximity interactome, which is also supported by the identification of previously characterized DYRK3 interactors during vesicular trafficking, centriolar satellite biogenesis and regulation of phase transitions of nuclear membrane-less organelles. This is the first reported study that unravel a link between DYRK3 and primary cilium and as such, this finding will provide important insight into the pathogenesis of the diseases linked to DYRK family kinases and the centrosome/cilium complex such as ciliopathies, primary microcephaly and cancer.

Given the extensive set of interactions identified in the DYRK3 proximity interactome, I was not able to pursue all the new relationships revealed by this map. To gain further insight into the regulation of the centrosome/cilium complex, I focused on further characterization of the relationship between DYRK3 and primary cilium. Future studies are required to validate first the new relationships for DYRK3 and then to investigate their functional implications. Interestingly, DYRK3 kinase dead list revealed more interactor proteins, in particular more proteins implicated in cilium assembly. In fact, this is consistent with the comparative analysis of the DYRK3 and DYRK3 KD physical interactome by GFP-pulldowns, which identified limited number of proteins due to the limitations of traditional approaches but still revealed a difference in the interactome landscape of DYRK3 and its KD mutant (Rai et al., 2018). These results suggest the exciting possibility that the kinase activity of DYRK3 might affect the stability or abundance of its direct or indirect targets in cells.

Using functional assays, I identified DYRK3 as a positive regulator of cilium assembly and cilium length regulation, but I note that my findings have not yet elucidated the molecular mechanism by which DYRK3 regulates ciliogenesis. Based on published studies, I propose two different mechanisms. First, DYRK3 might regulate cilium assembly and length via regulation of centriolar satellites. This is supported by studies that identify centriolar satellites as key regulators of cilium assembly and length as well as the relationship the reported regulatory relationship between DYRK3 activity and centriolar satellite's material state during its phase transitions in cell division (Conkar et al., 2019; Odabasi et al., 2019; Rai et al., 2018). In agreement, DYRK3-inhibited cells were disrupted for centriolar satellite organization, which was shown to be important for the ciliary functions of centriolar satellites (Aydin et al., 2020). This map revealed proximity interactions between DYRK3 and regulators of primary cilium assembly and function. The proximity interactors of DYRK3 included previously published interactors including centriolar satellite, vesicular trafficking, PML bodies, validating our approach. The proximity relationship of DYRK3 is in agreement with our hypothesis that it functions during cilium biogenesis and also suggests mechanisms by which DYRK3 regulates ciliogenesis. In order to increase the knowledge on DYRK3 regulation, validation of more centrosome/cilium complex interactors are required in the future

studies. The second possible mechanism is that DYRK3 might mediate its ciliary functions through the proteins identified in the DYRK3 interactome. For example, Kif7 stands out as a potential protein that might link DYRK3 to cilium length regulation. Like DYRK3 inhibition, Kif7 depletion results in longer cilia. Given its function as a microtubule depolymerase, Kif7 was reported to govern cilium length regulation via microtubule dynamics at the cilium tip (He et al., 2014). Future studies are required to distinguish between these two possible mechanisms or to unravel new mechanisms.

Notably, DYRK2 deletion was previously reported to result in increased cilium length via an AURKA-dependent mechanism (Yoshida et al., 2020). This suggests the possibility that cilium length regulation is a shared mechanism for Class II DYRKs. While my cellular assays provide important piece of data for uncovering this relationship, I also note that additional experiments should be performed in the future to strengthen this relationship. For example, I only elucidated the phenotypic consequence of DYRK3 inhibition using its kinase inhibitor. Given that the inhibitor might have off-target effects, acute depletion of DYRK3 by RNAi or chronic depletion by CRISPR/Cas9-genome editing approach will be required to validate the DYRK3-primary cilium relationship. The loss of function experiments have the potential to reveal a more specific understanding of DYRK3 function. In addition to cilium length regulation, DYRK2 was also studied for its functions during Hedgehog signaling via phosphorylation and degradation of GLI2 (Varjosalo et al., 2008). DYRK2's signaling function in the Hedgehog pathway suggests that DYRK3 might also have a function in this pathway. Hh signaling plays important role in embryonic development and requires primary cilia (Yoshida et al., 2020) and as such, pursuing this direction would be of interest to uncover disease mechanisms of DYRK3. I note that Hedgehog components were not enriched in the DYRK3 and DYRK3 KD proximity interactomes, which might be because the interactomes were generated form unciliated HEK293T cells.

To sum up, my findings identified DYRK3 as a new player of cilia biogenesis and advance our understanding of kinase-dependent regulation of this process. Future studies are required to elucidate the molecular mechanisms by which DYRK3 regulates primary cilium biogenesis and signaling.

CHAPTER 3: MATERIAL AND METHODS

3.1 Cell culture and transfection

RPE1 cells were cultured in DMEM/F12 50/50 medium supplemented with 10% fetal bovine serum (FBS, Life Technologies, Ref. # 10270-106, Lot # 42Q5283K) and 1% penicillin-streptomycin (P/S) (Pan Biotech, Cat. # P04-41250). HEK293T cells were cultured in DMEM supplemented with 10% FBS and 1% P/S (Pan Biotech, Cat. # P04-03590). All cells were cultured at 37 °C and 5% CO2. All cell lines were tested for mycoplasma by MycoAlert Mycoplasma Detection Kit (Lonza).

The plasmids were transfected into HEK293T cells using 1 g/l polyethylenimine, MW 25 kDa (PEI, Sigma-Aldrich, St. Louis, MO). The plasmids were diluted in Opti-MEM (Invitrogen) and treated with PEI at room temperature for 40 minutes. The cells were treated with the transfection mix for 48 hours, and immunofluorescence and immunoblotting were used to validate the expression of fusion proteins in transiently expressing cells.

For cilium assembly experiments, RPE1 cells were washed twice with PBS and incubated with DMEM/F12 supplemented with 1% P/S for the indicated times deprived FBS. For DYRK3 inhibition, cells were treated with 1 M GSK-626616 (Tocris Bioscience, Cat#6638).

3.2 MTEC Cultures

MTEC culture protocol was implemented as described in (Nanjundappa et al., 2019). MTECs are derived from wild-type BALB/C mice. Mice were sacrificed by CO_2 anesthesia and tracheas were surgically dissected. All work was approved by Koç University Animal Research Facility and Ethics Committee (2018.HADYEK.25).

Tracheas for MTEC cultures were dissected from male and female mice between 6-20 weeks of age wild- type BALB/C mice. The longitudinally cut trachea were incubated in 1.5 mg/ml pronase E in DMEM/F-12 supplemented with 1% penicillin-streptomycin (P/S) and incubated at 4°C overnight. The tube containing tracheal epithelial progenitor

cells were inverted by gentle agitation and collected in DMEM/F12 containing 10% FBS. After centrifugation at 4°C for 10 min at 800 g, cells were resuspended in DMEM/F12 with 10% FBS and plated in a Primaria Tissue Culture dish (Corning) for 3.5–4 hr at 37°C with 5% CO_2 to adhere contaminating fibroblasts. Non-adhered cells were collected, concentrated by centrifugation, resuspended in an appropriate volume of MTEC-complete medium and seeded at a density of 1×10^5 cells/cm^2 onto Transwell-Clear permeable filter supports (Corning) treated with 0.06 mg/ml rat tail Collagen type I. Air liquid interface (ALI) was introduced after cells reached confluence by feeding cells with MTEC serum-free medium only in the lower chamber (Mahjoub et al., 2010; Nanjundappa et al., 2019; Vladar & Stearns, 2007; You et al., 2002).

To inhibit DYRK3, cells were incubated in medium supplemented with 1 μM GSK-626616 (Tocris Bioscience, Cat#6638) beginning at 2 days after seeding. Cells were cultured at 37°C with 5% CO_2, and media containing GSK-626616 replaced every 2 days for up to 8 days. Filters were fixed at ALI days 0 and 8, fixed with cold Methanol.

3.3 Plasmids

pENTR_D_TOPO_WT (wild type) DYRK3 and pENTR_D_TOPO_KD (kinase dead) DYRK3 plasmids were gifts from Pelkmans Laboratory, University of Zurich. pDEST-Flag-BirA-DYRK3-WT and pDEST-Flag-BirA-DYRK3-KD (kinase dead) were cloned by Gateway recombination between N-Flag-BirA Backbone plasmid and the corresponding constructs.

3.4 Biotin-streptavidin affinity purification

HEK293T cells were cultured in 5x15 cm in DMEM media without antibodies (P/S) for the BioID experiment, and then transfected for 24 hours. The cells were cultured in media supplemented with 50 M biotin for 18 hours in the following day. Cells were lysed in BioID lysis buffer (50 mM Tris, pH 7.4, 500 mM NaCl, 0.4% SDS, 5 mM EDTA, 1 mM DTT, 2% Triton X-100, protease inhibitors PMSF, Aprotinin and LPC) after biotin incubation and sonicated. Insoluble material was pelleted after an equal amount of 4°C 50 mM Tris (pH 7.4) was added to the extracts. Streptavidin agarose beads were used to incubate soluble components from whole cell lysates (Thermo Scientific). Beads were collected and washed twice in wash buffer 1 (2% SDS in dH2O), once with wash buffer

2 (0.2% Deoxycholate, 1% Triton X-100, 500 mM NaCI, 1 mM EDTA, and 50 mM HEPES, pH 7.5), once with wash buffer 3 (10 mM Tris, pH 8.1, 250 mM LiCl, 0.5% NP-40, 0.5% Deoxycholate, 1% Triton X-100, 500 mM NaCl, 1 mM EDTA) and twice with wash buffer 4 (50 mM Tris, pH 7.4, and 50 mM NaCl). 10% of the sample was used for Western blot analysis and 90% of the sample to be analysed by mass spectrometry was washed once in 50 mM NH_4HCO_3. Confirmation of proximity interactors of DYRK3 was carried out by immunoblotting for FLAG antibody (Proteintech, DYKDDDDK tag Rabbit IgG Polyclonal antibody, Cat#20543-1-AP) that detect fusion protein and streptavidin that detect biotinylated proteins.

3.5 Immunofluorescence, microscopy, and quantitation

Cells were cultured on 24-well coverslips for immunofluorescence assays and treated in either 100% methanol or 4% paraformaldehyde in PBS for indirect immunofluorescence. After rehydration in PBS, cells were blocked with PBS + 0.1 percent Triton X-100 + 5% BSA (Sigma-Aldrich) (PBS-BT). Primary antibodies were diluted in blocking solution (PBS-BT). Anti-PCM1 antibody was generated and used for immunofluorescence as previously described (Firat-Karalar et al., 2014). Other antibodies used for immunofluorescence in this study were rabbit anti-PCM1 (homemade) at 1:4000, mouse anti-γ-tubulin (GTU-88; Sigma-Aldrich) at 1:1000, streptavidin (Life technologies), mouse anti-acetylated tubulin (AcTub, Santa Cruz Biotechnology, sc-23950) at 1:1000, mouse anti-ARL13B (NeuroMab, 75-287) at 1:500, mouse anti-polyglutamylated tubulin (GT335; Adipogen, A27791601) at 1:500, mouse anti-Centrin (Centrin 20H5, Milipore, 04-1624) at 1:1000, rat anti-ZO-1 (Santa Cruz Biotechnology, sc-33725) at 1:500. Antibodies used for western blotting were rabbit anti-PCM1 (homemade) at 1:4000, rabbit anti-Flag (Proteintech, 20543-1-AP) at 1:1000, mouse anti-vinculin (Santa Cruz Biotechnology, sc-55465), streptavidin (Invitrogen) at 1:10.000, rabbit anti-CEP131 (Bethyl Laboratories) at 1:1000, rabbit anti-GFP (homemade) at 1:1000 and rabbit anti-OFD1 (Proteintech, 22851-1-AP) at 1:1000. Following primary antibody incubation and 3X PBS wash, coverslips were incubated with Alexa Fluor 488-, 568-, or 633-conjugated secondary antibodies (Thermo Fisher) diluted in 1:2000 in blocking solution. Streptavidin linked to Alexa Fluor 488 or 594 was used to identify biotinylated proteins (Thermo Fisher). 4′,6-diamidino-2-phenylindole (DAPI; 1 g/ml) was used to stain DNA. Mowiol mounting media containing N-propyl gallate was used to mount the samples (Sigma-

Aldrich). Images were captured in 1024x1024 format with a step size of 0.5 m using the HC PL APO CS2 63x 1.4 NA oil objective with a Leica DMi8 inverted fluorescence microscope or SP8 scanning confocal microscope.

By obtaining a z stack of control and treated cells with equal gain and exposure conditions, quantitative immunofluorescence for DYRK3 was conducted. The z-stacks were used to assemble maximum-intensity projections. Maximum-intensity projections were assembled using z-stacks. The centrosome area of each cell was characterized using a centrosomal/basal body marker such as gamma-tubulin or acetylated tubulin. The centrosome/basal body region was defined as a 3 m^2 circle centered on the centrosome in each cell. ImageJ was used to calculate the total pixel intensity of PCM1 fluorescence within the region of interest. (National Institutes of Health, Bethesda, MD) (Schneider et al., 2012). The fluorescence intensity of a region of equal dimensions in the area closest to the centrosome was measured to perform background subtraction. These data were normalized to their mean for statistical analysis. Counting the total number of cells and the number of cells with primary cilia, as detected by DAPI and polyglutamated tubulin (GT335) and ARL13B staining, respectively, was used to measure primary cilium formation. Cilium length was assessed by measuring the length of the ARL13B signal in the LAS X Application in µm.

3.6 Ultrastructure Expansion Microscopy (U-ExM)

U-ExM was performed as previously described (Le Guennec et al., 2020). RPE1 cells were seeded on 24-well coverslips for control and DYRK3 inhibition conditions. When they became fully confluent, the cells are treated with serum starvation medium deprived FBS containing DMSO or 1 µM GSK-626616 for 24 hours. Coverslips were incubated in 1.4% formaldehyde (FA, 36.5–38%, F8775, SIGMA) / 2% acrylamide (AA, 40%, A4058, SIGMA) solution in 1X PBS for 5 h at 37 C prior to gelation in Monomer Solution supplemented with tetramethylethylendiamine (TEMED, 17919, ThermoFisher) and ammonium persulfate (APS, 17874, ThermoFisher) (final concentration of 0.5%) for 1 hr at 37°C. Denaturation was performed at 95°C for 1h30 and gels were stained with primary antibodies against mouse anti-polyglutamylated tubulin (GT335; Adipogen, A27791601) and mouse anti-acetylated tubulin (AcTub, Santa Cruz Biotechnology, sc-23950) at 1:500 for 3 h at 37 C. Gels were washed 3 X 10 min at RT with 1 X PBS with 0.1% Triton-X

(PBST) prior to secondary antibody incubation for 2h30 at 37 C followed by 3 X 10 min washes in PBST at RT. Gels were expanded in 3 X 150 ml dH2O before imaging.

3.7 Immunoprecipitation

EGFP-PCM1 and Flag-BirA constructs were co-transfected into HEK293T cells. Cells were washed and lysed with Flag Pulldown lysis buffer (50 mM HEPES, pH 8.0, 100 mM KCl, 2 mM EDTA, 10% Glycerol, 0.1% Nonidet™ P40, 1 mM DTT and protease inhibitors PMSF, Aprotinin and LPC) for 30 min after 48 hours of transfection. Lysates were centrifuged at 13.000 rpm for 15 min at 4ºC and supernatants were transferred to a new tube. 100 µl from each sample was saved as input. The rest of the supernatant was immunoprecipitated with Anti-FLAG M2 agarose beads (Sigma Aldrich) overnight at 4ºC. Then, beads were washed twice with lysis buffer, once with 0.1 M Glycin-HCl, pH 3.5, and 3X with lysis buffer. After washing, samples were resuspended in SDS containing sample buffer and immunoblotted.

3.8 Cell lysis and immunoblotting

Cells were lysed in 50 mM Tris-HCl, pH 7.5, 150 mM NaCl, 1 mM EDTA, 1 % Nonidet™ P40 and protease inhibitors PMSF, Aprotinin and LPC for 30 min at 4ºC followed by centrifugation at 13.000 g for 15 min. The Bradford solution was used to determine the protein concentration of the resultant supernatants (Bio-Rad Laboratories, CA, USA). Equal amounts of cell extracts were resolved on SDS-PAGE gels, transferred onto nitrocellulose membranes, and blocked with TBST in 5% milk for 1 hour at room temperature for immunoblotting. Primary antibodies diluted in 5% BSA in TBST were incubated overnight at 4°C on blots. The membranes were then washed three times with TBST for five minutes each time and blotted with secondary antibodies for one hour at room temperature in the following day. Blots were visualized with the LICOR Odyssey Infrared Imaging System and software at 169 mm after being washed three times with TBST for five minutes each time (LI-COR Biosciences). Primary antibodies used for immunoblotting were rabbit anti-PCM1 (Proteintech) at 1:1000, rabbit anti-Flag (Cell signaling,#2368) at 1:1000, mouse anti-vinculin (Santa Cruz Biotechnology, sc-55465) at 1:1000. Secondary antibodies used for western blotting experiments were IRDye680- and IRDye800-coupled and were used at 1:20.000 (LI-COR Biosciences).

3.9 Protein identification by Mass spectrometry

The on-bead tryptic digestion procedure was used for each sample to identify the biotinylated proteins by mass spectrometry at the Koç University Proteomics Facility (KUPAM), Istanbul, Turkey. Protein-bead complexes were washed with 8 M urea in 0.1 M Tris-HCl pH 8.5 solution, reduced with 100 mM DTT in urea solution for 45 minutes at 56°C, and alkylated with 50 mM iodoacetamide for 30 minutes at room temperature. The beads were washed with ammonium bicarbonate solution (50 mM NH4CO3) to eliminate the urea solution. 4 µg of trypsin (sigma cat no: T1426) was added to beads for an overnight digestion at 37°C for 600 µg of protein digestion. Peptides were desalted and eluted using C18 cartridges after being treated with 10% formic acid to stop trypsin digestion. Eluates were then dried in a speed vacuum system (Thermo Fisher Scientific cat no: SPD1010) and were analysed using a C18 nanoflow reversed-phase Dionex Ultimate 3000RSL liquid chromatography (Thermo Scientific, LC) system configurated with Q-Exactive Orbitrap mass spectrometer (Thermo Scientific, MS/MS). Samples were separated on an in-house packed 75 µm i.d. × 25 cm C18 column (Reprosil-Gold C18, 1.9 µm, 200 Å, Dr.Maisch) using 70 min linear gradients increasing from 5 to 40% acetonitrile in 0.1% formic acid with 300 nL/min flow in a 90 min total run time. The scan sequence is initiated with an MS1 spectrum (Orbitrap analysis; resolution 70 000; mass range 400−1500 m/z; automatic gain control (AGC) target 3e6; maximum injection time 60 ms). Up to 15 of the most intense ions per cycle were fragmented and analysed in the Orbitrap with data-dependent acquisition (DDA). Collision-induced dissociation (higher-energy collisional dissociation (HCD)) was used in the MS2 analysis (resolution 17 500; AGC 1e6; normalized collision energy (NCE) 26; maximum injection time 100 ms). The isolation window for MS/MS was 2.0 m/z. The human UNIPROT database version 2016 was used to search the data sets. Thermo Proteome Discoverer version 2.3 was used to identify proteins from raw files using the Sequest HT and Mascot search engines. Carbamidomethylation of cysteine was used as a fixed modification, and acetylation (protein N-termini) and oxidation of methionine were used as variable modifications. A maximum of two missed cleavages was allowed for the tryptic peptides. The peptide and protein false discovery rates (FDRs) were both set to 0.01 and the precursor mass tolerance was set to 10 ppm. The default settings were used for the other parameters.

3.10 Mass Spectrometry data analysis for BioID experiments

Raw data of two biological replicates for Flag-BirA*-DYRK3 wild type and kinase dead and two biological replicates for Flag-BirA* were analyzed by filtering non-specific proteins identified from experimental control sets as well as common MS/MS background proteins. I used Normalized Spectral Abundance Factor (NSAF) analysis to compare data from multiple runs and quantify the relative abundance of each proximity partner (Firat-Karalar et al., 2014). The normalized spectral counts were calculated by dividing each protein's spectral counts by the sum of all proteins' spectral counts. I calculated the ratio of normalized values of each protein in the Flag-BirA*-DYRK3 dataset relative to its normalized value in the Flag-BirA* dataset to separate generic interactors from particular ones. If the ratio was less than one, the protein was declared as contaminant. Finally, I used The Contaminant Repository for Affinity Purification – Mass Spectometry data (CRAPome) (Mellacheruvu et al., 2013) to reduce the most common mass spectrometry impurities. I used the CRAPome cut-off to eliminate proteins identified as contaminants in more than 200 of the 716 experiments. Finally, the remaining proteins were determined as the high-confidence DYRK3 interactors.

3.11 Network modelling and clustering analysis

The NSAF analysis retrieved 254 high confidence interactors of DYRK3 for WT, and 282 interactors for KD. Using the STRING database, I ran network analyses for the high confidence interactors (Szklarczyk et al., 2019), and Cytoscape 3.8.2 was used to visualize the network output file (Shannon et al., 2003). Proteins were grouped together based on their Go Ontology (GO) enrichments in cellular compartments, biological process, and molecular function to uncover overlapping complexes using the Clustering with Overlapping Neighborhood Expansion (ClusterONE) plug-in of Cytoscape (Nepusz et al., 2012). EnrichR, BioGrid (Oughtred et al., 2021), and DAVID (Huang et al., 2009) databases were used to determine the GO terms (Chen et al., 2013).

REFERENCES

Adams, N. A., Awadein, A., & Toma, H. S. (2009). The Retinal Ciliopathies. *http://Dx.Doi.Org/10.1080/13816810701537424*, *28*(3), 113–125.

Aranda, S., Laguna, A., & Luna, S. de la. (2011). DYRK family of protein kinases: evolutionary relationships, biochemical properties, and functional roles. *The FASEB Journal*, *25*(2), 449–462. https://doi.org/10.1096/FJ.10-165837

Arslanhan, M. D., Rauniyar, N., Yates, J. R., & Firat-Karalar, E. N. (2021). Aurora Kinase A proximity map reveals centriolar satellites as regulators of its ciliary function. *EMBO Reports*, e51902. https://doi.org/10.15252/EMBR.202051902

Aydin, Ö. Z., Taflan, S. O., Gurkaslar, C., & Firat-Karalar, E. N. (2020). Acute inhibition of centriolar satellite function and positioning reveals their functions at the primary cilium. *PLOS Biology*, *18*(6), e3000679. https://doi.org/10.1371/JOURNAL.PBIO.3000679

Bakre, A., Andersen, L. E., Meliopoulos, V., Coleman, K., Yan, X., Brooks, P., … Tripp, R. A. (2013). Identification of Host Kinase Genes Required for Influenza Virus Replication and the Regulatory Role of MicroRNAs. *PLOS ONE*, *8*(6), e66796. https://doi.org/10.1371/JOURNAL.PONE.0066796

Banani, S. F., Lee, H. O., Hyman, A. A., & Rosen, M. K. (2017). Biomolecular condensates: organizers of cellular biochemistry. *Nature Reviews Molecular Cell Biology 2017 18:5*, *18*(5), 285–298. https://doi.org/10.1038/nrm.2017.7

Banterle, N., & Gönczy, P. (2017). Centriole Biogenesis: From Identifying the Characters to Understanding the Plot. *Annual Review of Cell and Developmental Biology*, *33*(1), 23–49. https://doi.org/10.1146/annurev-cellbio-100616-060454

Bernhard, W., & Harven, E. de. (1960). L'ultrastructure du centriole et d'autres éléments de l'appareil achromatique. *Vierter Internationaler Kongress Für Elektronenmikroskopie / Fourth International Conference on Electron Microscopy / Quatrième Congrès International de Microscopie Électronique*, 217–227. https://doi.org/10.1007/978-3-642-49764-3_42

Bon, B. van, Hoischen, A., Hehir-Kwa, J., Brouwer, A. de, Ruivenkamp, C., Gijsbers, A., … Vries, B. de. (2011). Intragenic deletion in DYRK1A leads to mental retardation and primary microcephaly. *Clinical Genetics*, *79*(3), 296–299. https://doi.org/10.1111/J.1399-0004.2010.01544.X

Brooks, E. R., & Wallingford, J. B. (2014). Multiciliated cells: a review. *Current Biology : CB*, *24*(19), R973. https://doi.org/10.1016/J.CUB.2014.08.047

Chen, E., Tan, C., Kou, Y., Duan, Q., Wang, Z., Meirelles, G., … Ma'ayan, A. (2013). Enrichr: interactive and collaborative HTML5 gene list enrichment analysis tool. *BMC Bioinformatics*, *14*. https://doi.org/10.1186/1471-2105-14-128

Conkar, D., Bayraktar, H., & Firat-Karalar, E. N. (2019). Centrosomal and ciliary targeting of CCDC66 requires cooperative action of centriolar satellites, microtubules and molecular motors. *Scientific Reports 2019 9:1*, *9*(1), 1–17. https://doi.org/10.1038/s41598-019-50530-4

Conkar, D., Culfa, E., Odabasi, E., Rauniyar, N., Yates, J. R., & Firat-Karalar, E. N. (2017). The centriolar satellite protein CCDC66 interacts with CEP290 and functions in cilium formation and trafficking. *Journal of Cell Science*, *130*(8), 1450–1462. https://doi.org/10.1242/JCS.196832

Conkar, D., & Firat-Karalar, E. N. (2020). Microtubule-associated proteins and emerging links to primary cilium structure, assembly, maintenance, and disassembly. *FEBS Journal*, *288*(3), 786–798. https://doi.org/10.1111/febs.15473

Consortium, T. U., Bateman, A., Martin, M.-J., Orchard, S., Magrane, M., Agivetova, R., … Teodoro, D. (2021). UniProt: the universal protein knowledgebase in 2021. *Nucleic Acids Research*, *49*(D1), D480–D489. https://doi.org/10.1093/NAR/GKAA1100

Ferrante, M., Zullo, A., Barra, A., Bimonte, S., N, M., M, S., … Franco, B. (2006). Oral-facial-digital type I protein is required for primary cilia formation and left-right axis specification. *Nature Genetics*, *38*(1), 112–117. https://doi.org/10.1038/NG1684

Fırat-Karalar, E. N., & Stearns, T. (2014). The centriole duplication cycle. *Philosophical Transactions of the Royal Society B: Biological Sciences*, *369*(1650). https://doi.org/10.1098/RSTB.2013.0460

Fry, A. M., Sampson, J., Shak, C., & Shackleton, S. (2017). Recent advances in pericentriolar material organization: ordered layers and scaffolding gels. *F1000Research*, *6*, 1622. https://doi.org/10.12688/F1000RESEARCH.11652.1

Gambarotto, D., Zwettler, F. U., Le Guennec, M., Schmidt-Cernohorska, M., Fortun, D., Borgers, S., … Guichard, P. (2018). Imaging cellular ultrastructures using expansion microscopy (U-ExM). *Nature Methods 2018 16:1*, *16*(1), 71–74. https://doi.org/10.1038/s41592-018-0238-1

Gheiratmand, L., Coyaud, E., Gupta, G. D., Laurent, E. M., Hasegan, M., Prosser, S. L., … Pelletier, L. (2019). Spatial and proteomic profiling reveals centrosome-independent features of centriolar satellites. *The EMBO Journal*, *38*(14), e101109. https://doi.org/10.15252/EMBJ.2018101109

Hall, E., Keighren, M., Ford, M., Davey, T., Jarman, A., Smith, L., … Mill, P. (2013). Acute versus chronic loss of mammalian Azi1/Cep131 results in distinct ciliary phenotypes. *PLoS Genetics*, *9*(12). https://doi.org/10.1371/JOURNAL.PGEN.1003928

Hansen, G. M., Zambrowicz, B. P., Small, D., Vogel, P., Payne, B. J., Read, R. W., & Sands, A. T. (2011). Congenital Hydrocephalus in Genetically Engineered Mice. *Veterinary Pathology*, *49*(1), 166–181. https://doi.org/10.1177/0300985811415708

He, M., Subramanian, R., Bangs, F., Omelchenko, T., Liem, K. F., Jr., … Anderson, K. V. (2014). The Kinesin-4 Protein KIF7 Regulates Mammalian Hedgehog Signaling by Organizing the Cilia Tip Compartment. *Nature Cell Biology*, *16*(7), 663. https://doi.org/10.1038/NCB2988

Hildebrandt, F., Benzing, T., & Katsanis, N. (2011). Ciliopathies. *http://Dx.Doi.Org/10.1056/NEJMra1010172*, *364*(16), 1533–1543.

Hoh, R. A., Stowe, T. R., Turk, E., & Stearns, T. (2012). Transcriptional Program of Ciliated Epithelial Cells Reveals New Cilium and Centrosome Components and Links to Human Disease. *PLoS ONE*, *7*(12), 1–13. https://doi.org/10.1371/journal.pone.0052166

Hori, A, Barnouin, K., Snijders, A., & Toda, T. (2016). A non-canonical function of Plk4 in centriolar satellite integrity and ciliogenesis through PCM1 phosphorylation. *EMBO Reports*, *17*(3), 326–337. https://doi.org/10.15252/EMBR.201541432

Hori, Akiko, & Toda, T. (2016). Regulation of centriolar satellite integrity and its physiology. *Cellular and Molecular Life Sciences 2016 74:2*, *74*(2), 213–229. https://doi.org/10.1007/S00018-016-2315-X

Huang da, W., Sherman, B., & Lempicki, R. (2009). Systematic and integrative analysis of large gene lists using DAVID bioinformatics resources. *Nature Protocols*, *4*(1), 44–57. https://doi.org/10.1038/NPROT.2008.211

Ishikawa, H., & Marshall, W. F. (2011). Ciliogenesis: building the cell's antenna. *Nature Reviews Molecular Cell Biology 2011 12:4*, *12*(4), 222–234. https://doi.org/10.1038/nrm3085

Juhler, M. (2012). Animal models of hydrocephalus. *Adult Hydrocephalus*, 28–35. https://doi.org/10.1017/CBO9781139382816.004

Kawakami, M., Mustachio, L., Zheng, L., Chen, Y., J, R.-C., B, M., … Dmitrovsky, E. (2018). Polo-like kinase 4 inhibition produces polyploidy and apoptotic death of lung cancers. *Proceedings of the National Academy of Sciences of the United States of America*, *115*(8), 1913–1918. https://doi.org/10.1073/PNAS.1719760115

Kim, Kyeongmi, Lee, K., & Rhee, K. (2012). CEP90 Is Required for the Assembly and Centrosomal Accumulation of Centriolar Satellites, Which Is Essential for Primary Cilia Formation. *PLOS ONE*, *7*(10), e48196. https://doi.org/10.1371/JOURNAL.PONE.0048196

Kim, Kyeongmin, Lee, S., Kang, H., Shin, E., Kim, H. Y., Youn, H., & Youn, B. (2021). Dual Specificity Kinase DYRK3 Promotes Aggressiveness of Glioblastoma by Altering Mitochondrial Morphology and Function. *International Journal of Molecular Sciences 2021, Vol. 22, Page 2982*, *22*(6), 2982. https://doi.org/10.3390/IJMS22062982

Klos Dehring, D. A., Vladar, E. K., Werner, M. E., Mitchell, J. W., Hwang, P., & Mitchell, B. J. (2013). Deuterosome-Mediated Centriole Biogenesis. *Developmental Cell*, *27*(1), 103–112. https://doi.org/10.1016/J.DEVCEL.2013.08.021

Kodani, A., Yu, T. W., Johnson, J. R., Jayaraman, D., Johnson, T. L., Al-Gazali, L., … Reiter, J. F. (2015). Centriolar satellites assemble centrosomal microcephaly proteins to recruit CDK2 and promote centriole duplication. *ELife*, *4*(AUGUST2015). https://doi.org/10.7554/ELIFE.07519

Kubo, A., Sasaki, H., Yuba-Kubo, A., Tsukita, S., & Shiina, N. (1999a). Centriolar SatellitesMolecular Characterization, Atp-Dependent Movement toward Centrioles and Possible Involvement in Ciliogenesis. *Journal of Cell Biology*, *147*(5), 969–980. https://doi.org/10.1083/JCB.147.5.969

Kubo, A., Sasaki, H., Yuba-Kubo, A., Tsukita, S., & Shiina, N. (1999b). Centriolar SatellitesMolecular Characterization, Atp-Dependent Movement toward Centrioles and Possible Involvement in Ciliogenesis. *Journal of Cell Biology*, *147*(5), 969–980. https://doi.org/10.1083/JCB.147.5.969

Kubo, A., & Tsukita, S. (2003). Non-membranous granular organelle consisting of PCM-1: subcellular distribution and cell-cycle-dependent assembly/disassembly. *Journal of Cell Science*, *116*(5), 919–928. https://doi.org/10.1242/JCS.00282

Lauth, M., Bergström, A., Shimokawa, T., Tostar, U., Jin, Q., V, F., … Toftgård, R. (2010). DYRK1B-dependent autocrine-to-paracrine shift of Hedgehog signaling by mutant RAS. *Nature Structural & Molecular Biology*, *17*(6), 718–725. https://doi.org/10.1038/NSMB.1833

Le Guennec, M., Klena, N., Gambarotto, D., Laporte, M. H., Tassin, A.-M., Hoek, H. van den, … Guichard, P. (2020). A helical inner scaffold provides a structural basis for centriole cohesion. *Science Advances*, *6*(7), eaaz4137. https://doi.org/10.1126/SCIADV.AAZ4137

Lecland, N., & Merdes, A. (2018). Centriolar satellites prevent uncontrolled degradation of centrosome proteins: a speculative review. *Cell Stress*, *2*(2), 20–24. https://doi.org/10.15698/cst2018.02.122

Ma, F., Zhu, Y., Liu, X., Zhou, Q., Hong, X., Qu, C., … Zhang, Z. (2019). Dual-Specificity Tyrosine Phosphorylation–Regulated Kinase 3 Loss Activates Purine Metabolism and Promotes Hepatocellular Carcinoma Progression. *Hepatology*, *70*(5), 1785–1803. https://doi.org/10.1002/HEP.30703

Mahjoub, M. R., Xie, Z., & Stearns, T. (2010). Cep120 is asymmetrically localized to the daughter centriole and is essential for centriole assembly. *Journal of Cell Biology*, *191*(2), 331–346. https://doi.org/10.1083/JCB.201003009

Malicki, J. J., & Johnson, C. A. (2017). The Cilium: Cellular Antenna and Central Processing Unit. *Trends in Cell Biology*, *27*(2), 126–140. https://doi.org/10.1016/J.TCB.2016.08.002

Mao, J., Maye, P., Kogerman, P., Tejedor, F. J., Toftgard, R., Xie, W., … Wu, D. (2002). Regulation of Gli1 transcriptional activity in the nucleus by Dyrk1. *Journal of Biological Chemistry*, *277*(38), 35156–35161. https://doi.org/10.1074/jbc.M206743200

Marteil, G., Guerrero, A., Vieira, A., de Almeida, B., Machado, P., Mendonça, S., … Bettencourt-Dias, M. (2018). Over-elongation of centrioles in cancer promotes centriole amplification and chromosome missegregation. *Nature Communications*, *9*(1). https://doi.org/10.1038/S41467-018-03641-X

Mellacheruvu, D., Wright, Z., Couzens, A. L., Lambert, J.-P., St-Denis, N., Li, T., … Nesvizhskii, A. I. (2013). The CRAPome: a Contaminant Repository for Affinity Purification Mass Spectrometry Data. *Nature Methods*, *10*(8), 730. https://doi.org/10.1038/NMETH.2557

Mi, H., Muruganujan, A., Ebert, D., Huang, X., & Thomas, P. D. (2019). PANTHER version 14: more genomes, a new PANTHER GO-slim and improvements in enrichment analysis tools. *Nucleic Acids Research*, *47*(D1), D419–D426. https://doi.org/10.1093/NAR/GKY1038

Mirvis, M., Stearns, T., & James Nelson, W. (2018). Cilium structure, assembly, and disassembly regulated by the cytoskeleton. *The Biochemical Journal*, *475*(14), 2329–2353. https://doi.org/10.1042/BCJ20170453

Nachury, M., Loktev, A., Zhang, Q., Westlake, C., Peränen, J., A, M., … Jackson, P. (2007). A core complex of BBS proteins cooperates with the GTPase Rab8 to promote ciliary membrane biogenesis. *Cell*, *129*(6), 1201–1213. https://doi.org/10.1016/J.CELL.2007.03.053

Nakayama, K., & Katoh, Y. (2018). Ciliary protein trafficking mediated by IFT and BBSome complexes with the aid of kinesin-2 and dynein-2 motors. *The Journal of Biochemistry*, *163*(3), 155–164. https://doi.org/10.1093/JB/MVX087

Nanjundappa, R., Kong, D., Shim, K., Stearns, T., Brody, S. L., Loncarek, J., & Mahjoub, M. R. (2019). Regulation of cilia abundance in multiciliated cells. *ELife*, *8*. https://doi.org/10.7554/ELIFE.44039

Nepusz, T., Yu, H., & Paccanaro, A. (2012). Detecting overlapping protein complexes in protein-protein interaction networks. *Nature Methods 2012 9:5*, *9*(5), 471–472. https://doi.org/10.1038/nmeth.1938

Nigg, E. A., & Holland, A. J. (2018). Once and only once: Mechanisms of centriole duplication and their deregulation in diseases. *Nature Reviews Molecular Cell Biology*, *19*(5), 297–312. https://doi.org/10.1038/nrm.2017.127

Nigg, E. A., & Raff, J. W. (2009). Centrioles, Centrosomes, and Cilia in Health and Disease. *Cell*, *139*(4), 663–678. https://doi.org/10.1016/j.cell.2009.10.036

O'Roak, B., Vives, L., Fu, W., Egertson, J., Stanaway, I., Phelps, I., … Shendure, J. (2012). Multiplex targeted sequencing identifies recurrently mutated genes in autism spectrum disorders. *Science (New York, N.Y.)*, *338*(6114), 1619–1622. https://doi.org/10.1126/SCIENCE.1227764

Odabasi, E., Batman, U., & Firat-Karalar, E. N. (2020). Unraveling the mysteries of centriolar satellites: time to rewrite the textbooks about the centrosome/cilium complex. *Molecular Biology of the Cell*, *31*(9), 866–872. https://doi.org/10.1091/mbc.E19-07-0402

Odabasi, E., Gul, S., Kavakli, I. H., & Firat-Karalar, E. N. (2019). Centriolar satellites are required for efficient ciliogenesis and ciliary content regulation. *EMBO Reports*, *20*(6), e47723. https://doi.org/10.15252/EMBR.201947723

Oughtred, R., Rust, J., Chang, C., Breitkreutz, B., Stark, C., A, W., … Tyers, M. (2021). The BioGRID database: A comprehensive biomedical resource of curated protein, genetic, and chemical interactions. *Protein Science : A Publication of the Protein Society*, *30*(1), 187–200. https://doi.org/10.1002/PRO.3978

Pampliega, O., Orhon, I., Patel, B., Sridhar, S., Díaz-Carretero, A., Beau, I., … Cuervo, A. M. (2013). Functional interaction between autophagy and ciliogenesis. *Nature 2013 502:7470*, *502*(7470), 194–200. https://doi.org/10.1038/nature12639

Pimenta-Marques, A., & Bettencourt-Dias, M. (2020). Pericentriolar material. *Current Biology*, *30*, 677–697. https://doi.org/10.1016/j.cub.2020.04.064

Quarantotti, V., Chen, J.-X., Tischer, J., Tejedo, C. G., Papachristou, E. K., D'Santos, C. S., … Gergely, F. (2019). Centriolar satellites are acentriolar assemblies of centrosomal proteins. *The EMBO Journal*, *38*(14), e101082. https://doi.org/10.15252/EMBJ.2018101082

Rai, A. K., Chen, J. X., Selbach, M., & Pelkmans, L. (2018). Kinase-controlled phase transition of membraneless organelles in mitosis. *Nature*, *559*(7713), 211–216. https://doi.org/10.1038/s41586-018-0279-8

Reiter, J., & Leroux, M. (2017). Genes and molecular pathways underpinning ciliopathies. *Nature Reviews. Molecular Cell Biology*, *18*(9), 533–547. https://doi.org/10.1038/NRM.2017.60

Ricardo Bruno. (2017). Quantitative analysis of centriolar satellites and control of ciliogenesis by centrosome associated kinases - heiDOK. https://doi.org/https://doi.org/10.11588/heidok.00022944

Romio, L., Fry, A. M., Winyard, P. J. D., Malcolm, S., Woolf, A. S., & Feather, S. A. (2004). OFD1 Is a Centrosomal/Basal Body Protein Expressed during Mesenchymal-Epithelial Transition in Human Nephrogenesis. *Journal of the American Society of Nephrology*, *15*(10), 2556–2568. https://doi.org/10.1097/01.ASN.0000140220.46477.5C

Sanchez, A. D., & Feldman, J. L. (2017). Microtubule-organizing centers: from the centrosome to non-centrosomal sites. *Current Opinion in Cell Biology*, *44*, 93–101. https://doi.org/10.1016/J.CEB.2016.09.003

Scherft, J. P., & Daems, W. T. (1967). Single cilia in chondrocytes. *Journal of Ultrastructure Research*, *19*(5–6), 546–555. https://doi.org/10.1016/S0022-5320(67)80080-7

Shannon, P., Markiel, A., Ozier, O., Baliga, N., Wang, J., D, R., … Ideker, T. (2003). Cytoscape: a software environment for integrated models of biomolecular interaction networks. *Genome Research*, *13*(11), 2498–2504. https://doi.org/10.1101/GR.1239303

Singh, R., & Lauth, M. (2017). Emerging Roles of DYRK Kinases in Embryogenesis and Hedgehog Pathway Control. *Journal of Developmental Biology 2017, Vol. 5, Page 13*, *5*(4), 13. https://doi.org/10.3390/JDB5040013

Slepak, T. I., Salay, L. D., Lemmon, V. P., & Bixby, J. L. (2012). Dyrk kinases regulate phosphorylation of doublecortin, cytoskeletal organization, and neuronal morphology. *Cytoskeleton*, *69*(7), 514–527. https://doi.org/10.1002/CM.21021

Sluder, G. (2014). One to only two: a short history of the centrosome and its duplication. *Philosophical Transactions of the Royal Society B: Biological Sciences*, *369*(1650), 20130455. https://doi.org/10.1098/rstb.2013.0455

Sorokin, S. P. (1968). Reconstructions of Centriole Formation and Ciliogenesis in Mammalian Lungs. *Journal of Cell Science*, *3*(2), 207–230. https://doi.org/10.1242/JCS.3.2.207

Srsen, V., Fant, X., Heald, R., Rabouille, C., & Merdes, A. (2009). Centrosome proteins form an insoluble perinuclear matrix during muscle cell differentiation. *BMC Cell Biology 2009 10:1*, *10*(1), 1–9. https://doi.org/10.1186/1471-2121-10-28

Srsen, V., Gnadt, N., Dammermann, A., & Merdes, A. (2006). Inhibition of centrosome protein assembly leads to p53-dependent exit from the cell cycle. *Journal of Cell Biology*, *174*(5), 625–630. https://doi.org/10.1083/JCB.200606051

Stearns, T. (2004). The centrosome yields its secrets. *Nature Cell Biology 2003 6:1*, *6*(1), 14–14. https://doi.org/10.1038/ncb0104-14

Stubbs, J. L., Vladar, E. K., Axelrod, J. D., & Kintner, C. (2012). Multicilin promotes centriole assembly and ciliogenesis during multiciliate cell differentiation. *Nature Cell Biology 2012 14:2*, *14*(2), 140–147. https://doi.org/10.1038/ncb2406

Sun, S., Fisher, R. L., Bowser, S. S., Pentecost, B. T., & Sui, H. (2019). Three-dimensional architecture of epithelial primary cilia. *Proceedings of the National Academy of Sciences*, *116*(19), 9370–9379.

https://doi.org/10.1073/PNAS.1821064116

Szklarczyk, D., Gable, A., Lyon, D., Junge, A., Wyder, S., J, H.-C., … Mering, C. (2019). STRING v11: protein-protein association networks with increased coverage, supporting functional discovery in genome-wide experimental datasets. *Nucleic Acids Research*, *47*(D1), D607–D613. https://doi.org/10.1093/NAR/GKY1131

Tang, Z., Lin, M. G., Stowe, T. R., Chen, S., Zhu, M., Stearns, T., … Zhong, Q. (2013). Autophagy promotes primary ciliogenesis by removing OFD1 from centriolar satellites. *Nature 2013 502:7470*, *502*(7470), 254–257. https://doi.org/10.1038/nature12606

Tollenaere, M. A. X., Mailand, N., & Bekker-Jensen, S. (2015). Centriolar satellites: Key mediators of centrosome functions. *Cellular and Molecular Life Sciences*. Birkhauser Verlag AG. https://doi.org/10.1007/s00018-014-1711-3

Varjosalo, M., Björklund, M., Cheng, F., Syvänen, H., Kivioja, T., Kilpinen, S., … Taipale, J. (2008). Application of Active and Kinase-Deficient Kinome Collection for Identification of Kinases Regulating Hedgehog Signaling. *Cell*, *133*(3), 537–548. https://doi.org/10.1016/J.CELL.2008.02.047

Villumsen, B. H., Danielsen, J. R., Povlsen, L., Sylvestersen, K. B., Merdes, A., Beli, P., … Bekker-Jensen, S. (2013). A new cellular stress response that triggers centriolar satellite reorganization and ciliogenesis. *The EMBO Journal*, *32*(23), 3029–3040. https://doi.org/10.1038/EMBOJ.2013.223

Vladar, E. K., & Stearns, T. (2007). Molecular characterization of centriole assembly in ciliated epithelial cells. *Journal of Cell Biology*, *178*(1), 31–42. https://doi.org/10.1083/JCB.200703064

Wang, L., Failler, M., Fu, W., & Dynlacht, B. D. (2018). A distal centriolar protein network controls organelle maturation and asymmetry. *Nature Communications 2018 9:1*, *9*(1), 1–15. https://doi.org/10.1038/s41467-018-06286-y

Wang, L., Lee, K., Malonis, R., Sanchez, I., & Dynlacht, B. D. (2016). Tethering of an E3 ligase by PCM1 regulates the abundance of centrosomal KIAA0586/Talpid3 and promotes ciliogenesis. *ELife*, *5*(MAY2016). https://doi.org/10.7554/ELIFE.12950

Waters, A. M., & Beales, P. L. (2011). Ciliopathies: an expanding disease spectrum. *Pediatric Nephrology 2011 26:7*, *26*(7), 1039–1056. https://doi.org/10.1007/S00467-010-1731-7

Wei, L., Sun, J., Guo, J., Zhan, R., Mi, X., & Li, M. (2018). Aquaporin 4 Silencing

Aggravates Hydrocephalus Induced by Injection of Autologous Blood in Rats. *Medical Science Monitor*, *24*, 4204–4212. https://doi.org/10.12659/msm.906936

Wilkinson, C. J., Carl, M., & Harris, W. A. (2009). Cep70 and Cep131 contribute to ciliogenesis in zebrafish embryos. *BMC Cell Biology 2009 10:1*, *10*(1), 1–14. https://doi.org/10.1186/1471-2121-10-17

Winey, M., & O'Toole, E. (2014). Centriole structure. *Philosophical Transactions of the Royal Society B: Biological Sciences*, *369*(1650). https://doi.org/10.1098/rstb.2013.0457

Wippich, F., Bodenmiller, B., Trajkovska, M. G., Wanka, S., Aebersold, R., & Pelkmans, L. (2013). Dual specificity kinase DYRK3 couples stress granule condensation/ dissolution to mTORC1 signaling. *Cell*, *152*(4), 791–805. https://doi.org/10.1016/j.cell.2013.01.033

Woodruff, J. B., Wueseke, O., & Hyman, A. A. (2014). Pericentriolar material structure and dynamics. *Philosophical Transactions of the Royal Society B: Biological Sciences*, *369*(1650). https://doi.org/10.1098/RSTB.2013.0459

Yoshida, S., Aoki, K., Fujiwara, K., Nakakura, T., Kawamura, A., Yamada, K., … Yoshida, K. (2020). The novel ciliogenesis regulator dyrk2 governs hedgehog signaling during mouse embryogenesis. *ELife*, *9*, 1–29. https://doi.org/10.7554/ELIFE.57381

You, Y., Richer, E. J., Huang, T., & Brody, S. L. (2002). Growth and differentiation of mouse tracheal epithelial cells: selection of a proliferative population. *https://Doi.Org/10.1152/Ajplung.00169.2002*, *283*(6 27-6).